Renewable and Sustainable Energy Reviews 213 (2025) 115473

Contents lists available at ScienceDirect

Renewable and Sustainable Energy Reviews

journal homepage: www.elsevier.com/locate/rser

A review of technology, applications, and future perspectives of thermosyphons in permafrost regions

Yinghong Qin [a], Shima Yazdani [b], Fanghua Li [c], Mikhail Sheremet [b], Mohammad Ghalambaz [d,b,*]

[a] College of Civil Engineering and Architecture, Guangxi Minzu University, 188 University Road, Nanning, Guangxi, 530006, China
[b] Laboratory on Convective Heat and Mass Transfer, Tomsk State University, Tomsk, Russia
[c] College of Civil Engineering and Architecture, Guangxi University, 100 University Road, Nanning, Guangxi, 530004, China
[d] Department of Mathematics, Saveetha School of Engineering, SIMATS, Chennai, India

ARTICLE INFO

Keywords:
Thermosyphons
Permafrost preservation
Heat transfer
Working fluid
Cold climate engineering
Infrastructure stability

ABSTRACT

Thermosyphons, utilizing natural convection and phase change mechanisms, offer a reliable and maintenance-free solution for heat transfer, crucial for preserving permafrost and maintaining infrastructure stability. This paper reviews the design variations and operational principles of thermosyphons, highlighting their adaptability and effectiveness in diverse applications such as transportation, energy, and infrastructures in Earth regions with low temperature. Over the past decades, the cooling performance of thermosyphons, especially two-phase closed thermosyphons, has been widely employed to save permafrost subgrades under pavements, railway embankments, pipeline foundations, transmission tower foundations, buildings, and other structures in Northern America, Russia, China, and elsewhere. These applications have been the focus of numerical simulations, laboratory experiments, and field studies. Recent innovations, including the use of nanorefrigerants, new configurations such as L-shaped and horizontal thermosyphons, and the combination of thermosyphons with other passive cooling technologies, have significantly improved their performance and efficiency. Some innovative applications, however, remain at the stage of laboratory research, numerical simulations, or conceptual modeling, with further field studies needed to assess their durability, reliability, and ease of construction. This review underscores the importance of continued research to enhance material durability, operational efficiency, and the development of advanced monitoring systems.

Nomenclature

<!–Col Count:4–>Symbols

A	Amplitude of temperature variation, °C	f	Frozen
B	Phase shift in temperature variation, °C	g	Ground
C	Mean annual surface temperature, °C	i	Ice
C_s	Specific capacity	s	Soil
d_0	Outside diameter of the TPCT, m	u	Unfrozen
F	Thermal exchange area, m^2		
FI	Freezing index	Greek Symbols	
FN	Frost number	α	Convective thermal energy transport, W/(m^2·°C

(*continued on next column*)

(*continued*)

h	Thawed ground thickness, m	β_i	Ratio of ice content to unfrozen moisture content
H	Height above ground for wind velocity measurement, m	θ	Volumetric moisture
L	Latent heat of vaporization, kJ/kg	λ_a	Thermal conductivity of air, W/(m·K)
l	Length of the evaporation zone, m	ρ	Density, kg/m^3
N_{ua}	Nusselt number for fluid	v_{10}	Wind velocity at 10 m above ground, m/s
P	Pressure, Pa		
Q	Heat flux, W	Abbreviations	
R	Total thermal resistance, K/W	COP	Coefficient of Performance
R_1, R_2, … R_6	Specific thermal resistances, K/W	CRCOP	China-Russia Crude Oil Pipeline

(*continued on next page*)

* Corresponding author.
E-mail addresses: yqin1@mtu.edu (Y. Qin), shima.yazdaani@gmail.com (S. Yazdani), rzhangcug@gmail.com (F. Li), sheremet@math.tsu.ru (M. Sheremet), m.ghalambaz@gmail.com (M. Ghalambaz).

https://doi.org/10.1016/j.rser.2025.115473
Received 13 September 2024; Received in revised form 6 January 2025; Accepted 6 February 2025
Available online 14 February 2025

(*continued*)

S	Permafrost thaw settlement parameter	FR	Filling Ratio
S_r	Relative degree of saturation of frozen soil	GWP	Global Warming Potential
T	Temperature, °C	HTPCT	Horizontal Two-Phase Closed Thermosyphon
TI	Thawing index	LTPCT	L-shaped TPCT
ΔT	Temperature difference, °C	ODP	Ozone Depletion Potential
		QTH	Qinghai-Tibet Highway
Subscripts		TPCT	Traditional Two-Phase Closed Thermosyphon
a	Air	VCRS	Vapor Compression Refrigeration System
e	Evaporator		

1. Introduction

Thermosyphons are a crucial component in thermal management technologies, enabling the passive transfer of heat through natural convection and phase change mechanisms. These systems do not require mechanical pumps, making them highly reliable and cost-effective, especially in permafrost regions where maintaining electrically driven cooling devices is challenging and expensive. At the core of a thermosyphon's operation is a self-sustaining cycle where heat is absorbed by the working medium in the evaporator area, causing it to vaporize. The vapor rises to the condenser area, releases thermal energy to the surroundings, and condenses back into a fluid, which gravity then returns to the evaporator, completing the cycle. This efficient, energy-independent process is vital for preserving permafrost and maintaining the structural integrity of infrastructure in cold climates.

Thermosyphons are essential for the protection and maintenance of permafrost, which underlies vast regions including Siberia, Alaska, Northern Canada, China, and elsewhere. These devices play a pivotal role in safeguarding infrastructure, such as the Qinghai-Tibet Railroad (QTR), from the detrimental effects of global warming, which promotes permafrost thaw and compromises the structural integrity of the ground, thereby endangering the reliability and safety of critical structures [1]. Thermosyphons facilitate the removal and dissipation of ground heat, maintaining a stable, frozen state of the permafrost, which is critical for the longevity of overlying systems like roads, buildings, and pipelines [2]. Their use also extends to broader protection against frost damage and temperature variations, enhancing energy efficiency through their passive operational mode [2]. Examples such as their use in the Alaska Pipeline project and the Qinghai-Tibet Railway highlight the effectiveness of thermosyphons in maintaining infrastructure stability under challenging permafrost conditions [3]. They ensure stable and level surfaces for safer transportation by keeping the permafrost layer frozen. Additionally, thermosyphons are deployed in various infrastructure projects across permafrost regions, including pipelines, railway embankments, and utility poles, where they mitigate risks associated with thermal expansion and contraction that could lead to leaks or ruptures [4–6]. The deployment of thermosyphons in permafrost infrastructure offers multiple benefits, including high heat transfer efficiency and effective stability management with minimal environmental impact. They are adaptable to various soil conditions and infrastructure types, providing a versatile solution for permafrost areas. Their effective utilization requires precise design and strategic placement, taking into account local soil characteristics, permafrost properties, and anticipated thermal demands.

Research on the use of thermosyphons to preserve permafrost subgrades beneath infrastructure in cold regions has expanded significantly, encompassing laboratory studies, numerical simulations, and conceptual modeling [7,8]. This growing body of work highlights the need for a comprehensive review to examine the various dimensions of thermosyphons, including their theoretical foundations, operational mechanisms, and technological advancements. This paper provides a comprehensive examination of empirical studies and practical implementations of thermosyphons designed for cold environments, emphasizing key advancements that have improved their efficiency, reliability, and range of applications [9–19]. By assessing various applications, this paper addresses challenges such as optimizing thermal efficiency, improving material durability, and minimizing environmental impacts. Finally, the review suggests future research directions and potential interdisciplinary collaborations that could further optimize and expand the use of thermosyphons in cold regions [20–24].

2. Thermosyphons technology

2.1. Types of thermosyphons

Thermosyphons are categorized based on their configuration and the mechanism facilitating the fluid's return. Taking into account the coolant motion direction, thermosyphons can be classified into two main groups, namely, two-phase thermosyphons and loop thermosyphons.

As shown in Fig. 1(a), two-phase closed thermosyphons (TPCTs) resemble regular tubes without an internal wick structure. In operation, the coolant absorbs heat in the evaporator, causing it to vaporize. This vapor goes to the condenser and it releases heat and condenses back into a fluid. Gravity then returns the liquid to the evaporator, necessitating that the condenser be installed in a higher place than the evaporator for effective functioning. Consequently, the condenser must be set up higher compared to the evaporator for the thermosyphon to function effectively; horizontal installation renders it inoperative [25]. This vertical orientation allows TPCTs to transport the thermal energy efficiently from the lower part to the upper one, making them suitable for applications such as cold energy storage systems [26]. They utilize phase change dynamics to transport the thermal energy effectively across surfaces having minimal temperature difference, proving invaluable in geo-temperature regulation within permafrost areas [27–29].

Loop thermosyphons, also known as separated heat pipes [30,31] or thermosyphon loops [32,33], consist of an evaporator, condenser, fluid pipe (down-comer) [34], and vapor pipe (raiser) [35]. In these systems, the evaporator and condenser are separate and connected by the liquid and vapor pipes, as illustrated in Fig. 1(b–d). The liquid-filled space between the evaporator and condenser can be either partially or fully filled; the flow from the evaporator to the condenser can consist of vapor alone or a mixture of vapor and liquid. During operation, the coolant absorbs heat in the evaporator and vaporizes. The vapor goes through the vapor pipe to the condenser due to buoyancy forces, carrying some liquid upward due to viscosity forces. Inside the condenser, the vapor condenses back into liquid, which then returns to the evaporator along the liquid pipe. Closed-loop systems are highly efficient for applications requiring precise thermal management and are particularly effective in scenarios like electronic cooling [36–38], and enhancing heat exchanger efficiency in cold climates [39–41]. Also, a closed-loop system can be used to cool permafrost subgrade by deploying the evaporation section as horizontal pipes filled with working fluid and placing these pipes beneath the permafrost base of the infrastructure [42]. In contrast, open-loop thermosyphons are not completely sealed, allowing the integration and replenishment of the working medium, either vapor or liquid, from external sources as shown in Fig. 1(f) [43]. This configuration is advantageous for systems requiring fluid top-ups or integration with larger environmental mechanisms, such as geothermal heating or snow melting systems, providing flexibility and adaptability to varying thermal conditions [44,45]. The outlet is typically positioned at a higher elevation than the inlet to ensure that the working medium flows in the desired direction (Fig. 1(f)) [46]. Open-loop thermosyphons are typically preferred for large-scale projects due to their fluid management flexibility [47]. An open thermosyphon features a closed tubular bar functioning as the evaporator and an open end leading to a container acting as the condenser. This design allows for the integration and

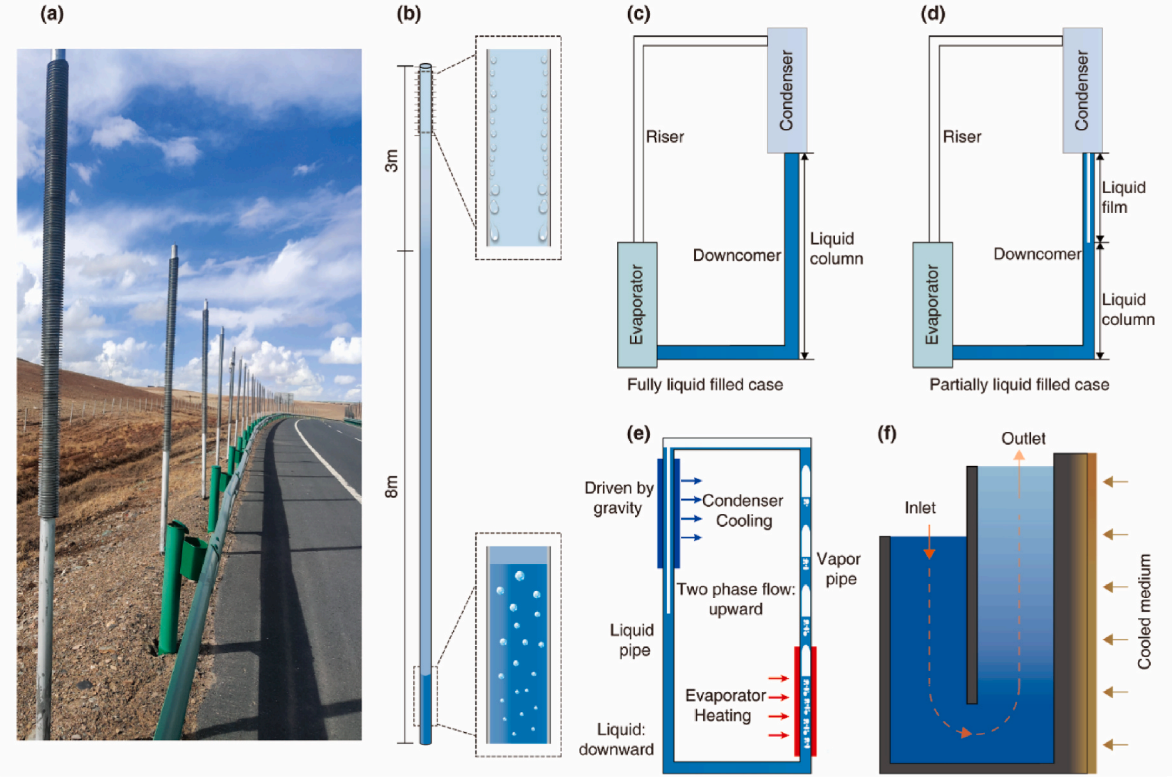

Fig. 1. Schematic of typical thermosyphons; (a) A row of thermosyphons installed along a road (b) the evaporation and condensing of two-phase closed thermosyphon; (c) Closed-loop thermosyphons with the liquid-filled space filled fully, (d) Closed-loop thermosyphons with the liquid-filled space partially fully, (e) Closed-loop thermosyphons with the motion from the evaporator to the condenser consist of a mixture of vapor and liquid, (f) Open-loop thermosyphon, adapted from [46].

replenishment of fluid from external sources, making them highly adaptable for various thermal applications. Low-density thermal energy recovery, solar water heating, gas turbine blade cooling, and nuclear reactor cooling are some examples of open-loop thermosyphon utilization [48]. Open-loop thermosyphons are seldom used in cooling permafrost subgrade, possibly because the open section of the thermosyphon is difficult to maintain routinely, given the harsh weather conditions that make accessing permafrost regions challenging.

2.2. Operation principles

Thermosyphons operate through the application of thermodynamics and fluid mechanics, efficiently transporting heat across spatial gradients without necessitating external energy inputs. Central to their function is the phase change of the working medium, a process that significantly enhances the thermal energy transfer capabilities owing to the substantial latent thermal energy of vaporization involved. The operation of a thermosyphon is described using two primary phenomena: the thermal energy transport and the phase change of the working medium. Within the evaporator area, situated at the lower end and exposed to a heat source, the temperature of the working fluid escalates until it achieves its boiling point under the pressure in the closed-loop structure. At this juncture, the fluid undergoes a phase transition from liquid to vapor, absorbing the heat from the surrounding – referred to as the latent thermal energy of vaporization. This transformation is pivotal, facilitating a more efficient regime of the thermal energy transport compared to conduction or convection alone. As the vapor, now lighter than its liquid counterpart, rises to the cooler condenser area at the upper part of the thermosyphon, it encounters a cooler surface. This contact induces the vapor to condense, transforming back into a liquid and releasing the thermal energy previously absorbed during vaporization. The heat released during this process is dissipated into the surrounding environment or into a designated cooling medium, as depicted in Fig. 1 (b) [49]. Following condensation, the denser liquid flows back to the evaporator by the gravitational force, and as a result completing the thermal energy transport cycle.

The boiling point, which is affected by the thermal flux and medium properties, is a critical factor that depends on the saturation temperature and pressure of the working medium [50]. In a thermosyphon, the pressure can vary along the system's height and locally affect the boiling point. For example, at the higher pressures found in the deeper parts of the thermosyphon, the fluid's boiling point will be higher. The interaction between temperature and pressure is critical to its operation in a closed system such as a thermosyphon [51].

2.3. Design and components

Thermosyphons, while simple in design, feature three main elements, including the evaporator, the adiabatic area, and the condenser. The evaporator, placed at the lower part, initiates the thermal energy transport phenomenon by absorbing thermal energy and vaporizing the working fluid. In cold climates, the evaporator's design may incorporate materials with high thermal conductivity or fins to enhance heat absorption [27].

The adiabatic area is as a thermal bridge, insulated to prevent heat loss and ensure the vapor reaches the condenser without premature condensation. This section's length and insulation are critical, particularly in cold regions, to maintain the system's thermal efficiency. The condenser, positioned at the top, facilitates heat release and vapor condensation, often enhanced with features like fins to increase the heat transfer area [52]. In colder settings, modifications might include materials or coatings to prevent frost buildup and facilitate continuous operation under freezing conditions.

Environmental factors such as the inclination angle of the thermosyphon, wind speed, and ambient temperature critically influence its cooling efficacy. Design adjustments in cold regions may include

additional insulation in the adiabatic area to decrease the thermal energy loss and the use of materials like stainless steel or titanium for enhanced durability and corrosion resistance [53].

Incorporating thermal storage systems enables these thermosyphons to store excess heat, which can be crucial during periods of low heat demand or ambient temperatures. This capability ensures continuous thermal management and enhances the system's efficiency in cold environments. As indicated in Table 1, it is recommended to maintain a spacing of approximately 3.0 m between thermosyphons to optimize their radius of influence and ensure effective heat dissipation [54–56]. These design strategies are significant for maximizing the performance and reliability of thermosyphons in challenging thermal conditions.

Jin et al. [56] conducted an extensive research on the cooling performance of various thermosyphon configurations in permafrost Earth areas. Their findings revealed that for traditional TPCT spaced 12 m apart, the cooling effect is primarily concentrated at the shoulder of the embankment, achieving a cooling radius of approximately 3 m. The L-shaped TPCT configuration improves cooling in the core of the embankment, creating a low-temperature area of −1.5 °C with a cooling radius of about 5 m from the evaporators' endpoints. However, this configuration is less effective on the slopes, potentially leading to permafrost degradation [57]. To weaken the impact of radiation on slopes, L-shaped TPCT is best used in company having slope cooling measures like crushed-rock revetment [58,59].

The Horizontal Thermosyphon (HTPCT) exhibits superior overall cooling performance compared to the other configurations. The HTPCT achieves a cooling radius of approximately 7 m [56], measured from the midpoint between two HTPCTs. It ensures a more uniform temperature distribution across the embankment, reducing transverse temperature differences and enhancing embankment stability [60]. These results indicate that while traditional TPCTs provide localized cooling, both L-shaped TPCT and HTPCT configurations offer improved and more uniform cooling over a larger radius. The HTPCT, in particular, excels in managing overall temperature distribution and maintaining embankment integrity in permafrost regions [56]. Research on the cooling performance of HTPCP is still primarily limited to laboratory studies and numerical simulations, highlighting the need for further field experiments to validate the permafrost cooling effects observed in these simulations.

2.4. Working fluid in thermosyphons

Refrigerants, capable of undergoing phase transitions at both low and high temperatures, are integral to various applications including refrigeration systems, space engineering systems, and the preservation of blood, medication, and food [61]. In thermosyphons, the choice of material and working medium is critical, particularly for low-temperature applications [62]. The performance of thermosyphons relies heavily on selecting an appropriate working fluid within a sealed system to facilitate heat transfer through natural convection, eliminating the need for mechanical assistance [63–65]. Recent studies have explored various types of coolants used in thermosyphon systems, categorized into three main groups: inorganic coolants, Freon refrigerants, and other organic coolants. Table 2 summarizes the refrigerant specifications used by past researchers in thermosyphon fields [66–68].

Water and carbon dioxide (R744) are the examples of inorganic coolants. CO_2 is particularly notable for its environmental friendliness and significant energy-saving potential, boasting a higher thermal energy transport capability in comparison to many other coolants. However, using CO_2 presents challenges. It operates at much higher pressures than Freon refrigerants, has a critical temperature close to the upper operating limits of data center racks, and requires stringent safety measures to prevent leakage due to its high working pressure. Water, on the other hand, is a cost-effective and environmentally benign option. Unlike most coolants, which operate at pressures above atmospheric levels, water operates below atmospheric pressure, making the system prone to air ingress, which can degrade heat transfer efficiency. Addressing leaks in water systems is cumbersome as it requires complete drainage, vacuuming, and refilling of the system to restore optimal performance. Freon refrigerants category includes R22, R134a, R410A, and others. R22, while non-flammable and non-toxic, is being phased out due to its ozone-depleting properties. R134a, which has replaced R22 in many applications, offers a balance of lower working pressure and higher thermal energy transport ability. R410A provides even higher heat transfer efficiency but operates at higher pressures and has a complex composition that can affect performance if leakage occurs. R32, similar in pressure to R410A, offers good heat transfer performance but is flammable, posing safety risks in industrial applications. Despite their effectiveness, Freon refrigerants generally have high global warming potential (GWP), contributing to their classification as greenhouse gases with poor environmental performance. Other organic coolants include n-pentane and HFE7000. Fluorocarbons, known for their stability, large latent thermal energy, and non-conductivity, are also used in engineering applications. While fluorocarbons are stable and effective for immersed cooling techniques [25], their potential use in loop thermosyphons warrants further study to understand their full capabilities and limitations.

The chosen working fluid must match the application's operational temperature ranges. The compatibility of the medium with the working material, as well as the fluid's boiling point, is paramount [69,70]. For low-temperature uses, ammonia and refrigerants like R134a, R22, and R410a are preferred due to their favorable thermodynamic properties, and are often employed in conjunction with compatible shell materials such as copper, steel, and aluminum [65,71–75]. Ammonia is often used as a coolant in thermosyphons designed to preserve permafrost due to its favorable thermodynamic properties. Ammonia has a high latent thermal energy of vaporization and operates effectively at low temperatures, making it ideal for maintaining the subfreezing conditions required to preserve permafrost. However, ammonia's toxicity and potential environmental risks necessitate careful design and monitoring to prevent leaks and ensure safe operation (Table 2).

2.4.1. Filling ratio of the working fluids

The filling ratio (FR) is a crucial characteristic that significantly impacts the thermal energy transport efficiency of loop thermosyphons. The FR represents the proportion of the coolant volume changed by the loop thermosyphon relative to the overall volume, which can be defined either as the volume of the evaporator [85] or the overall volume of the loop thermosyphon [86]. When the total volume is determined as the evaporator volume, the FR can exceed 100 %, whereas it remains below 100 % when considering the entire loop volume. The FR directly influences the coolant's condition, affecting whether it is superheated or overcooled, which in turn impacts the system's thermal energy transport capability. The optimal FR, where no superheating or overcooling forms, is termed the best filling ratio and is essential for the efficient regime of the thermosyphon [85]. Thermosyphons operate under three primary conditions based on the FR: the dry-up limit, the best filling ratio, and the flood limit [87–89]. At the dry-up limit, a low FR and high heat flux cause the upper evaporator section to dry out, reducing the thermal energy transport efficiency owing to a shift in the motion pattern [90]. At the best filling ratio, the coolant remains in a saturated state in both the evaporator and condenser, facilitating optimal thermal energy transport conditions. Conversely, at the flood limit, the condenser's

Table 1
Effective cooling radius for various thermosyphon configurations.

Type of Thermosyphons	Cooling Radius (m)	Refs.	Method
TPCT	3	[54–56]	Exp.
L-shaped TPCT	5	[56]	Exp.
HTPCT	7	[56]	Exp.

Table 2
Specifications of commonly used refrigerants in thermosyphons.

Cooling Fluid	Refs.	Boiling Temperature (°C)[a]	GWP	Viscosity (μPa.s)		Density (kg /m³)		Advantage and Disadvantage
				Liquid	Vapor	Liquid	Vapor	
R134a	[66–68]	−26.07	1430 [76]	384.2	9.68	1376.7	5.26	Nonflammable, no ozone depletion potential (ODP), high global warming potential (GWP). Environmentally friendly substitute for R-12 and R-22. Commonly employed in refrigerators and automotive air conditioning systems.
R22	[68]	−40.81	1810 [76]	346	9.75	1409.2	4.7	Good heat transfer properties and efficiency, high ODP, being phased out due to environmental concerns.
R410A	[68]	−51.44	2088 [77]	346.4	9.9	1349.7	4.17	Excellent efficiency, used in residential and commercial air conditioning. No ODP but relatively high GWP.
R404A	[68]	−46.22	3922 [78]	328.5	9.13	1306.3	5.48	Widely used in commercial refrigeration. No ODP but high GWP. Blend of R125, R143a, and R134a, offering good low-temperature performance.
R407C	[68]	−43.63	1624 [79]	384.6	9.98	1380.7	4.63	Used in air conditioning systems. No ODP and moderate GWP. Blend of R32, R125, and R134a, providing similar performance to R22 but with lower environmental impact.
R12	[68]	−29.75	10900 [76]	345.2	9.56	1487	6.29	High molecular weight and lower heat transfer coefficient. Nonflammable but high ODP and GWP.
R32	[66,68]	−51.7	677 [80]	276.7	9.26	1212.9	2.99	High heat transfer coefficients, lowest normal boiling point. Low flammability, no ODP, and a component of R407C. Reasonably high GWP.
R600a	[66,68, 81]	−11.75	3 [82]	227.8	6.58	593.8	2.83	Commonly used in freezers, especially in northern Europe. Minimal ODP and low GWP, making it environmentally friendly.
Water	[83,84]	100	0	281.8	12.27	958.4	0.6	Very low vapor pressure, requiring larger diameter pipes. Safe and environmentally friendly.
Ammonia	[66,68]	−33.33	0	255.5	8.05	682	0.89	Ammonia provides efficient, cost-effective, and environmentally friendly heat transfer but is toxic, flammable, corrosive, and requires stringent safety measures and regulatory compliance.

[a] Boiling temperature in this table is the boiling temperature at standard air pressure.

bottom becomes submerged in liquid, leading to overcooling and decreased heat transfer efficiency. Research by Ding et al. [91] presented that filling ratios limit the thermal energy transport. The filling ratio does not influence the thermal energy transport within the evaporator or the total thermal energy transport capacity of the loop thermosyphon as long as the heat transfer process is not restricted.

Research by Payakaruk et al. [92] demonstrated that the filling ratio does not significantly impact the thermal energy flow ratio across various orientations, including vertical alignments. However, Wang and Ma [93] found that the optimal inclination angle for heat pipes, ranging between 20° and 50°, is influenced by the filling ratio. Their experiments with 10 %, 23 %, and 33 % liquid fillings showed that lower liquid fill rates increase the condensation coefficient.

Emami et al. [94] reported maximum thermal energy transport efficiency at a 60° inclination for various aspect ratios and filling rates, noting that a 35 % tilt was particularly effective. Elmosbahi et al. [95] observed optimal heat transfer performance when the methanol volume was about two-thirds of the evaporation area's volume, indicating the essential impact of the filling ratio on functionality. In cold regions like Alaska, the FR's effect on low-temperature heat transfer performance remains underexplored [96]. Observations suggest that during hibernate periods, the liquid ammonia level within heat pipes ranges from 0.3 to 0.6 m, indicating that fluid levels rise with boiling-induced gas generation. This variation is likely correlated with temperature differences between the evaporation and condensation ends, although dynamic studies are lacking. A 65 % liquid filling intensity at low temperatures has been obtained to result in the lowest thermal resistance at a 20° inclination [96]. Zhang et al. [97] studied a heat pipe having a 65 % liquid filling strength at low temperatures and revealed the lowest overall heat resistance at a 20° inclination angle.

In Table 3, a summary of studies conducted on working fluid effects on thermosyphon heat transfer characteristics is provided; Different refrigerants also exhibit varying efficiencies based on the FR. Hydrofluorocarbons (HFC) refrigerants like R134a and R404a perform better at specific fill ratios, while R407c shows reduced efficiency under similar conditions [98]. The heat transfer coefficients for ethanol closely match established correlations for over-filled conditions [99]. Further investigations by Ma et al. [81] and subsequent analyses by Ong et al. [100], Jeong [101], and Ong and Haider-E-Alahi [67] explored various operational variables like fill ratios and coolant flow rates, demonstrating their impact on performance. Ma et al. [81] conducted an investigation into the performance of various working fluids in solar TPCTs. Their study highlighted the mixture of R245fa/R152a as demonstrating superior thermal performance, achieving higher temperature increases, greater efficiency, and increased heat flow rates, all while maintaining lower operational pressures compared to R134a. Additionally, the working fluids R1234ze, R600a, and R245fa were found to offer lower temperature increases and pressures, underscoring their environmental advantages due to their lower global warming potential. Payakaruk et al. [92] and Terdtoon et al. [102,103] utilizing R123 refrigerants assessed the impact of aspect ratio and orientation on ther thermal energy transport, finding that certain configurations could significantly enhance efficiency. As the working fluid was nitrogen, Nakano et al. [104] demonstrated that vapor-liquid interactions on the evaporator wall were critical to optimal heat transfer.

2.4.2. Nanorefrigerants utilization in thermosyphons

Table 4 presents a summary of studies indicating that Nanorefrigerants have been shown to enhance boiling and condensing processes more effectively compared to pure refrigerants. Nanorefrigerants offer an alternative method to enhance thermosyphon performance [106]. Additionally, incorporating nanoadditives in refrigerants substantially rises the pressure difference, that benefits thermosyphon operation. Sun and Yang [107] studied how nanorefrigerants affect heat transfer in internal thread copper tubes. They were especially interested in how different mass fractions of nanoparticles affect heat transfer improvements. They reported that the heat transfer coefficient increased by 17 %–25 % across various setups, with the Cu-R141b nanorefrigerant exhibiting the highest enhancement of up to 25 %. Mahbubul et al. [108–111] have extensively studied the impact of nanoparticle volume concentration on the thermophysical properties and heat transfer performance of nanorefrigerants. They highlighted the benefits of Al_2O_3/R-134a and Al_2O_3/R141b nanorefrigerants in improving thermal conductivity and heat transfer coefficients, especially at higher particle concentrations and temperatures. Specifically, their findings demonstrate that the thermal conductivity of Al2O3/R141b nanorefrigerant

Table 3
Summary of effect of using various working fluids on heat Transfer characteristics in thermosyphons.

Researchers	Cooling Fluid	Findings
Gorecki [98]	R134a, R407c and R404a	R134a and R404A exhibited the highest thermal energy transport intensities. Optimal fill ratio for both refrigerants was 10 %. R407C runs at rather high pressures, which is a drawback in thermosyphon systems. R407C's performance was 50 % below. Using this refrigerant also has certain disadvantages in terms of rather high working pressures and a 30 % optimal filling ratio.
Lataoui and Jemni [99]	water, acetone, and ethanol	Overfilled thermosyphon results align with Imura's correlation. Importance of controlling input heat flux and cooling fluid temperature for optimal performance.
Ma et al. [81]	R134a, R601, R245fa, R600a, R1234ze, R152a, R245fa/R152a, and R601/R245fa	R245fa/R152a mixture achieved a heat transfer rate higher than that of R134a and R245fa by 4.46 % and 19 %, respectively.
Ong and Haider-E-Alahi [67]	R-134a	Performance increased with higher fill ratios and greater temperature difference between the bath and condenser section. The maximum heat transfer achieved was approximately 750 $W/m^2 \cdot K$ for a fill ratio of 0.35, and around 1750 $W/m^2 \cdot K$ for a fill ratio of 0.8, with a coolant mass flow rate of 0.0121 kg/s.
Ong et al. [100]	R410A	Thermal energy transport resistance and overall performance were independent of fill ratio and inclination angle. Lower aspect ratio thermosyphons had higher heat transfer resistance, resulting in lower thermal performance consistent with results for water, R410A, and R134a.
Jeong [101]	CO_2	The maximum heat transfer rate is reached when the heat transfer flux is roughly 3000 W/m^2 for all fluid ratios (0.07–0.9). Evaporator section thermal energy transport coefficient was approximately two times higher compared to Kutateladze's correlation. Condenser section heat transfer coefficients aligned well with the Nusselt equation.
Payakaruk et al. [92]	R134a, R22, water, and ethanol	Working fluid properties significantly affected the heat transfer ratio. The modified Kutateladze number effectively predicted the maximum thermal energy transport ratio and minimum overall heat resistance ratio. The maximum angle for the heat transfer ratio compared to the vertical position ($Q_{max} = Q_{90}$) occurs between 40 and 60°.
Terdtoon et al. [102]	R123	Internal flow patterns change with aspect ratio and inclination. At an aspect ratio of 10 and higher, inner motion varies from annular and churn motion at the vertical location to stratified slug motion at the inclined location.
Nakano et al. [104]	Nitrogen	Maximum thermal energy transport strength is defined by the interaction between vapor motion and returning liquid film flow along the evaporator wall. Temperature difference between evaporator and condenser becomes constant above 100 K.
Abou-Ziyan et al. [65]	Water, R134a	Combination of 350 mm adiabatic length and 0.5 fill ratio provided the highest output thermal flux. The water-copper thermosyphon's performance tends to be reduced by 5 %–20 % below the boiling limit due to vibration. On the other hand, throughout the tested range of input heat flux, vibration improves performance at the beginning of the boiling limit by almost the same ratio. Below the boiling limit, R134a exhibits little to no effect, but above the boiling limit, an enhancement of up to 250 % takes place.
Solomon et al. [105]	R600a, R290	The anodization process improved the evaporator's thermal energy transport coefficient by up to 33 % at a 45° inclination angle with an input of 200 W. In comparison to the non-anodized TPCT, the TPCT's total thermal resistance decreased by 17 %, 20 %, and 23 % for horizontal, inclined, and vertical positions, respectively.

increases with both the augmentation of particle concentrations and the rise in temperature. In contrast, viscosity also increases with particle volume but decreases with increasing temperature, affecting the flow and pressure drop characteristics essential for system design and efficiency. In the study conducted by Kedzierski and Gong [112] the influence of CuO nanoparticles added to R134a refrigerant was examined to assess enhancements in pool boiling heat transfer. The research demonstrated that the introduction of CuO nanoparticles into the R134a/polyolester mixture significantly increased the boiling heat transfer rates. For a nanolubricant mass fraction of 0.5 %, an enhancement in the heat transfer rate of between 50 % and 275 % was observed compared to pure R134a/polyolester mixtures. The study by Henderson et al. [113] studied the impact of SiO2 and CuO nanoparticles dispersed in R-134a and R-134a/polyolester (POE) mixtures was analyzed for their influence on flow-boiling heat transfer. The experiments revealed that adding SiO2 nanoparticles directly to R-134a resulted in a decrease in the heat transfer coefficient by as much as 55 %, likely due to the challenges in achieving a stable nanoparticle dispersion. In contrast, excellent dispersion was achieved with CuO nanoparticles in a mixture of R-134a and POE, which significantly increased the heat transfer coefficient, more than doubling it over baseline results with just R-134a/POE. Jiang et al. [114] highlighted the potential of carbon nanotubes to significantly enhance the thermal conductivity of refrigerants, with R113 as the base fluid. The study found that optimizing the diameter and aspect ratio of CNTs could lead to thermal conductivity enhancements of up to 104 %. While these results are promising for improving energy efficiency in refrigeration systems, the environmental impact of using a high-GWP refrigerant such as R113 remains a concern. This underscores the need for future research to explore similar enhancements using refrigerants with lower GWP, thereby ensuring that environmental sustainability is maintained alongside technological advancements. In their experimental investigation, Sabareesh et al. [115] studied what happened when TiO2 nanoparticles were added as a

Table 4
Overview of inclusion of nano particles with refrigerant in thermosyphon applications.

Researchers	Method	Cooling Fluid	Findings
Sun and Yang [107]	Exp.	Cu/R141b, Al/R141b, Al_2O_3/R141b, CuO/R141b	A significant rise in the heat transfer coefficient was noted for Cu-R141b nanorefrigerant, with a maximum increase of 25 %.
Mahbubul et al. [108]	Num.	Al_2O_3/R-134a	Thermal conductivity increased with higher particle fraction and temperature but reduced with larger particle sizes. Significant increment in heat transfer coefficient with higher nanoparticle volume fractions.
Mahbubul et al. [109–111]	Num.	Al_2O_3/R141b	Optimal nanoparticle concentrations can significantly improve refrigeration system performance by balancing enhanced heat transfer with manageable pressure drops and energy requirements.
Kedzierski and Gong [112]	Exp.	R134a/CuO	An improvement in the heat transfer rate between 50 % and 275 % was noted for a nanolubricant mass fraction of 0.5 % over pure R134a/polyolester mixtures.
Henderson et al. [113]	Exp.	R-134a/SiO_2, CuO	Direct dispersion of SiO_2 nanoadditives in R-134a resulted in up to a 55 % decrease in heat transfer coefficient. Excellent dispersion of CuO nanoadditives in R-134a/polyolester oil led to a heat transfer coefficient increase of over 100 % compared to baseline R-134a/POE results.
Jiang et al. [114]	Exp.	R113/CNT	Up to 104 % thermal conductivity increases could result from optimizing CNT diameters and aspect ratios.
Sabareesh et al. [115]	Exp.	R12/TiO_2	Results showed that a 0.01 % volume fraction reduced compressor work by 11 % and increased heat transfer by 3.6 %. The COP increased by 17 % after adding nanoparticles to the lubricating oil.
Diao et al. [116]	Exp.	R141b–SDBS/Cu	Presence of Cu nanoparticles and SDBS surfactant significantly improved heat transfer performance.
Akhavan-Behabadi et al. [117]	Exp.	R600a/oil/CuO	Addition of CuO nanoparticles to the baseline mixture significantly enhanced heat transfer, with a maximum enhancement of 83 % observed for the nanorefrigerant with a 1.5 % mass fraction.

lubricant to vapor compression refrigeration systems that used R12 as the coolant. The experimental results showed that a 0.01 % volume fraction lowered the average compressor work by roughly 11 % and raised the average heat transfer rate by roughly 3.6 %. The addition of nanoparticles to the lubricating oil ultimately led to a 17 % increase in the COP. The study highlights the potential of nanoparticle additives to improve energy efficiency, although it does not delve into the environmental implications of using a high GWP refrigerant like R12. This gap suggests a need for further research into how nanoparticle-enhanced lubricants might be used with lower GWP refrigerants to achieve both efficiency gains and environmental benefits. Diao et al. [116] investigated the effects of nanoparticle addition on the pool boiling performance and critical heat flux of Cu-R141b nanorefrigerants. The study demonstrated that the addition of copper nanoparticles and the surfactant SDBS to R141b improves the pool boiling heat transfer performance. Akhavan-Behabadi et al. [117] looked at how heat moved through a horizontal tube when R600a was mixed with polyolester oil (POE) and CuO nanoparticles. The experiments demonstrated that the addition of a 1.5 % mass fraction of CuO nanoparticles resulted in an 83 % increase in the heat transfer rate compared to pure refrigerant. Notably, the study utilizes R600a, an environmentally friendly refrigerant with a low global warming potential, aligning the technological advancements with sustainability goals. This combination of low-GWP refrigerant and nanoparticle technology presents a compelling case for the future development of refrigeration systems that are both efficient and have minimal environmental impact.

Although many researchers have conducted experimental studies on thermosyphons, monitoring internal pressure and velocity remains challenging. Accurate observations of these parameters are crucial for predicting the behavior of the working medium within the thermosyphon. Developing a device capable of measuring pressure and velocity inside thermosyphons poses a significant challenge and provides motivation for future research in this field.

3. Applications of thermosyphons

3.1. Field applications

Thermosyphons and heat pipes have been effectively employed across a variety of fields due to their superior heat transport capabilities and operational reliability [118]. Key applications include space systems, cold regions, the automotive industry, railroads, the electrical and electronics industries, and the nuclear industry.

Since 1960, thermosyphons have been integrated in stabilizing foundations in permafrost regions, with notable usage in Alaska, where over 900 instances were recorded by 2008 [119]. It has been widely used to keep roadway subgrades frozen (Fig. 2 (a)), cool the permafrost beneath building foundations (Fig. 2(b)–and (c)), cool concrete poles of transmission towers in permafrost regions (Fig. 2(d)–and (e)), and preserve the permafrost surrounding the support rods for pipelines (Fig. 2 (f)–and (g)). The largest deployment occurred with the Trans-Alaska Pipeline, which utilized approximately 120,000 units [120]. This technology has been concurrently developed and applied in several countries including the US, Canada, China, and Russia, beginning as early as the 1970s in China and the 1990s in Russia [121–123].

In practical applications, thermosyphons have proven crucial for maintaining the stability of the Trans-Alaska Pipeline System. This system employs thermosyphons integrated with vertical support beams and insulation to effectively manage the thermal effects on permafrost, ensuring long-term structural integrity [13]. Similarly, thermosyphons are widely utilized in civil and mining projects in Canada [124]. In 1978, the first at-grade building on ice-rich permafrost was constructed at Ross River, Yukon Territory, using thermosyphons for subgrade cooling [125]. These thermosyphons had an evaporator slope of 10 %, which inspired the construction of similar structures in the Prudhoe Bay and Kuparuk oilfields in the subsequent years [6]. In the 1980s and early 1990s, a sloping evaporator thermosyphon system, initially installed in 1982, was used to build numerous at-grade buildings and heated tanks in the oilfields [6]. Notable examples include the Inuvik Hospital, which utilized these devices to expedite ground freezing processes and enhance the efficacy of partially damaged passive thermosyphons at the Female Young Offender Facility in the Northwest Territories [42]. They were also employed to protect the frozen ground at Simon Allaituq School in Nunavut, which had been influenced by heat supply lines.

Furthermore, thermosyphons have been used to construct

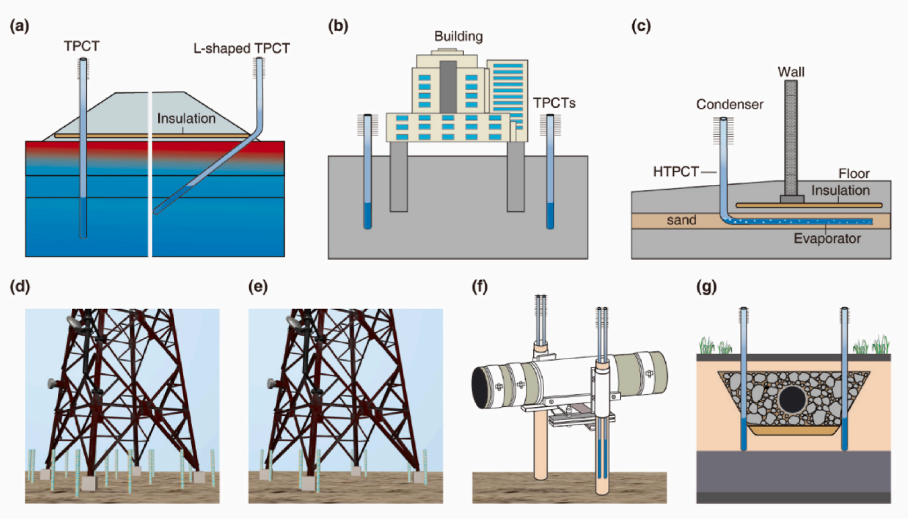

Fig. 2. Schematic diagram illustrating the application of TPCT for cooling in various infrastructure settings: (a) Roadway embankment, (b–c) building subgrade, (d–e) transmission tower piles, and (f–g) pipeline supporting pods.

containment walls for tailings dams and mining sites in cold regions [40]. The design of the dam incorporated thermosyphons after significant thawing was observed, which contributed to the dam's instability. In the case study of the Kubaka Gold Mine in the Russian Far East, thermosyphons were not initially utilized during the construction and early operation of the dam [126]. This oversight led to unexpected thawing and structural problems. It was only after monitoring the dam's performance and noting excessive movement and seepage that the decision was made to retrofit the dam with thermosyphons. The findings from this implementation emphasize the importance of integrating thermosyphons into the initial design phase of infrastructure projects in cold regions. This adaptation was essential to prevent further degradation of the dam's integrity, reflecting a reactive approach to environmental management in cold-region mining operations. Hayley et al. [127] studied using thermosyphons at the EKATI Diamond Mine to maintain the structural integrity and functional stability of dams constructed on permafrost. The finding demonstrated that this technology is essential for keeping the core and foundation of these dams below critical temperature thresholds, preventing thawing that could cause structural failures or loss of dam integrity. Additionally, the Diavik Diamond Mine incorporated thermosyphons in constructing mine dams and the Lac De Gras dikes to accelerate ground freezing [42,124].

In the Russian railway projects, particularly those traversing the permafrost regions of Yakutia, innovative technologies have been utilized to combat the challenges posed by the harsh climate conditions and the thaw-sensitive nature of the soil [128]. One significant technology implemented is the use of thermosyphons, which are integral to maintaining the structural integrity and operational stability of railway subgrades in these ice-rich permafrost areas [129]. The Tommot-Nizhny Bestyakh Railway section, situated between kilometer posts 692 and 734, exemplifies the strategic placement of thermosyphons in conjunction with insulation materials such as Penoplex boards [130]. These measures are critical for controlling the thermal regime beneath the railway embankments and preventing the degradation of permafrost beneath the tracks. The embankment designs have included specific configurations like vertical thermosyphons placed along the berms of low embankments and insulated snow sheds on the slopes, which help in mitigating the heat transfer from the embankment to the underlying permafrost. Monitoring studies [131], provide data that these technologies effectively lower ground temperatures and stabilize the permafrost table beneath the railway infrastructure. This is crucial for ensuring the longevity and reliability of the railway operations in such extreme environments, where thermal instability can lead to significant structural failures.

Thermosyphons also have been used to preserve the permafrost subgrade of the China-Russia Crude Oil Pipeline (CRCOP). A schematic representation of this application is shown in Fig. 2(f-g). Recent research on the CRCOP highlights the critical role of thermosyphons in mitigating thaw settlement issues in permafrost regions [132]. The CRCOP has experienced significant subsidence issues over the last decade due to the increasing temperature of the oil being transported, which causes the permafrost close to the pipeline to thaw. These challenges pose risks to pipeline integrity and stability due to the changing thermal regime of the surrounding permafrost. Extensive on-site monitoring around the CRCOP showed that the seasonal thawing depth (STD) is about 11 m in 2022 [132]. Laboratory experiments complemented these findings by demonstrating how thermosyphons could erase the thaw bulb around the pipeline, leading to decreased STD. In another study, the combined experimental and numerical approaches demonstrated the efficacy of thermosyphons in stabilizing pipeline foundations in permafrost regions, offering valuable insights for future applications and layout optimization [133]. The study concluded that the most efficient performance was achieved with longer evaporator sections and shorter spacing between thermosyphons.

Further afield, in the Qinghai-Tibet Plateau, extensive use of thermosyphons in the Qinghai-Tibet Railway embankment over a 34-km stretch demonstrates their effectiveness in lowering ground temperatures and managing permafrost conditions [24]. The thermosyphons can be vertically inserted from the shoulder of the embankment into the underlying permafrost (Fig. 2(a), the left part of (a)) or installed from the embankment shoulder with a bend L-shaped inward to the soil beneath the center of the embankment (Fig. 2 (a), the right part of (a)). Installation of L-shaped thermosyphons is technically challenging and costly, a difficulty often overlooked in past literature, with most studies on L-shaped thermosyphons remaining conceptual or experimental. To enhance cooling, a crushed-rock revetment on the embankment shoulder, along with other passive cooling techniques, can be employed to further improve the cooling efficiency of an embankment equipped with a TPCT. Another approach is to install a thermosyphon, with the evaporator section horizontally positioned at the bottom (Fig. 2 (c)).

Field studies confirm their efficacy in stabilizing permafrost, with optimal spacing and orientation enhancing their performance [134–139]. Additionally, research by Guan-fu et al. [140] into the thermal characteristics of TPCTs under varying climatic conditions reveals their potential and highlights regional effectiveness differences, underscoring the need for optimization to local climates and soil

characteristics. These applications showcase thermosyphons' broad utility and adaptability across a range of engineering challenges in cold climates.

Song et al. [141] conducted an extensive evaluation of TPCT used to cool embankments along the QTH, situated in permafrost regions. Utilizing eight years of monitoring data from 2004 to 2011, the research assessed the impact of thermosyphons on stabilizing permafrost and reducing thaw-related infrastructure damage. Findings revealed that embankments equipped with thermosyphons maintained lower ground temperatures and exhibited a more stable permafrost table compared to traditional embankment structures. Also, there are many similar studies that highlights the significant advantages of using thermosyphons for enhancing the durability and stability of infrastructure in permafrost-affected areas [58,142–155].

Traditional Two-Phase Closed Thermosyphons (TPCTs) are typically installed vertically into the shoulders or toes of embankments. To enhance the cooling performance at the embankment center, the evaporator area of TPCTs can be angled, creating what is known as an L-shaped TPCT. Scientists have investigated the cooling efficacy of L-shaped TPCTs through both experimental and numerical simulation [58,59,153,156,157]. Their studies indicate that this configuration significantly cools the permafrost beneath the embankment center, thereby improving its stability. However, longitudinal cracks often develop in highway embankments equipped with TPCTs [141,143].

Several studies have identified that these cracks are primarily caused by the lateral geotemperature difference induced during the cooling process by TPCTs [156,158]. The frost heave around embankments with TPCTs is significantly greater than those without, leading to secondary structural issues and reduced stability. Although measures such as ripped-rock revetments, shading boards, and temperature-controlled ventilation ducts can mitigate differential geotemperature distribution to some extent [159–161], their effectiveness diminishes over time due to factors such as snow or sand clogging the crushed-rock layers [162], environmental damage to shading boards [163], and heat transfer inefficiencies in the soil between ventilation ducts during warm seasons [164].

To address these challenges, Pei et al. [147] studied a self-adapting horizontal thermosyphon method, which effectively balances asymmetric geotemperature distributions. However, the central section of the embankment tends to experience increased temperatures under high ambient conditions due to the inherent working characteristics of this system. The issue of permafrost stability in highways remains unresolved, especially as expressway pavements are approximately twice as wide as standard highways, leading to a 60 % growth of the mean annual thermal flux at the embankment base [165].

Jin et al. [56] explored the use of Horizontal Thermosyphon (HTPCT) in permafrost areas, installing TPCTs centrally in the embankment and HTPCTs at the base on both sides. This setup potentially cools the underlying permafrost over a size of up to 35 m. In terms of construction, TPCT installation in permafrost regions requires drilling depths of 8 m or more, which is both costly and inefficient when combined with crushed rock. Conversely, HTPCT installation is more straightforward and economical, as the evaporator area can be laid horizontally on the soil layer post-roadbed foundation treatment, with an insulation board placed above for added efficiency. This method eliminates the need for additional reinforcement measures.

The increased horizontal cooling range of HTPCTs makes them ideal for linear infrastructure projects such as embankments, oil pipelines, and tunnels. Their use can significantly diminish the number of required TPCTs without compromising the cooling influence. Given the substantial heat accumulation in expressways, construction of separate embankments for inflow and outflow lanes might be the optimal approach to mitigate this issue. However, this construction increases land use and alters air motion and underground hydrological processes close to the embankment, potentially destabilizing the structure and affecting the efficiency of engineering measures.

Table 5 provides a summary of the studies conducted in this field. Detailed descriptions of these researches are presented in the following parts.

3.2. Experiment studies

The study of thermosyphons in permafrost regions has yielded a wealth of knowledge. Various experiments have demonstrated their effectiveness in maintaining soil stability and preventing thaw-induced damage. This section summarizes key experimental studies, illustrating the innovative use of thermosyphons across different settings and their significant contributions to infrastructure stability.

In Western Siberia, Bayasan et al. [167] introduced innovative two-phase heat pipes having enlarged heat-exchange surfaces to improve the heat stability of permafrost soils beneath buildings and structures. These thermostabilizers with improved productivity (TIP) featured extra fins on condensers and dual plating on evaporators, outperforming traditional heat pipes like the TMD-5 model. TIP models with an equivalent diameter of 160 mm achieve a frozen soil radius of 1.56 m in Pangody and 1.44 m in Surgut. Focusing on infrastructure in China, Chen et al. [168] and Zhang et al. [142] evaluated thermosyphon technology along the Chaidaer-Muli Railway. Chen's team installed thermosyphons over a 20 km stretch, resulting in a more stable roadbed structure. Zhang's in-situ tests further validated the cooling effects of TPCTs, demonstrating their ability to stabilize the permafrost table and enhance soil stability in both warmer and ice-rich regions. Wu et al. [143] assessed the thermal performance of TPCT embankments along the QTH using experimental data collected from 2004 to 2012. The study site, located on the Chu Kumar River Plain, features ice-rich permafrost and an average elevation exceeding 4400 m. Their findings revealed that the TPCTs transferred between 47.6 W and 63.5 W instantaneously, with peak performance observed during cold time owing to the greater temperature drop between the air and the ground. The TPCT's cooling effect exhibited dynamic changes over the years, with higher energy transfer rates initially, followed by a gradual stabilization.

In 1982, Bethel Airport in Alaska completed the first installation of thermosyphons on a runway [169]. A total of 31 thermosyphons were placed on the east shoulder of the runway [170]. On the west shoulder, the evaporator sections of the thermosyphons extended almost horizontally, with a slope of 15:1 beneath the runway. Researchers analyzed the performance of the thermosyphons by examining the soil temperatures around the units [166]. The operational thermosyphons at Bethel Airport significantly reduced the temperature of the subbase, which strengthened and stabilized that section of the runway. This was one of the first successful installations on an embankment with thermosyphon units that were almost horizontal. Enhancements and advancements in thermosyphon installations for embankments are a focus of continuous research. Lai et al. [58] investigated the innovative use of L-shaped thermosyphons and crushed-rock revetments and insulation to stabilize embankments in permafrost regions. Their laboratory tests simulated real-world embankment conditions, constructing a scaled embankment with specific configurations of L-shaped thermosyphons in a controlled environment to replicate permafrost conditions. The results were compelling: the L-shaped thermosyphons significantly enhanced cooling effectiveness deep within the embankment compared to traditional methods. This configuration demonstrated a remarkable ability to keep heat stability and prevent thaw settlement of the underlying permafrost, showcasing its potential for broader application in cold region infrastructure.

Building on the exploration of thermosyphon applications, Guo et al. [144] delved into the challenges of frost jacking in pile foundations caused by closed thermosyphons in seasonally frozen or thawed permafrost regions. Focusing on a tower foundation along the Qinghai-Tibet power transmission line, they observed that while TPCTs effectively cool foundation soil and enhance structural stability, they

Table 5
Summary of studies on TPCT Technique and their findings.

Ref.	Study Location	Applications	Method	Findings
[127]	EKATI Diamond Mine	Thermosyphons	Exp.	Thermosyphons can keep the dams' core and foundation below critical temperatures to prevent thawing and structural failure.
[126]	Kubaka Gold Mine	Thermosyphons	Exp.	The results of this implementation highlight the importance of incorporating thermosyphons into the initial design phase of infrastructure projects in cold regions.
[132]	CRCOP	Pipeline	Exp.	Thermosyphons mitigated thaw settlement problems in permafrost regions of the CRCOP.
[133]	CRCOP	Stabilizing pipeline foundation	Num.	Permafrost along the CRCOP can be thermally stabilized with thermosyphons.
[141]	QTH	Embankment	Exp.	TPCTs maintain lower ground temperatures and stable permafrost table compared to traditional methods.
[142]	Chaidaer-Muli Railway	Embankment	Exp.	TPCTs-inserted embankments effectively cooled permafrost and raised the permafrost table in marshy regions.
[143]	QTH	Embankment	Exp.	TPCTs embankment transferred 1500–2000 MJ of energy annually, with peak performance during cold seasons.
[58]	Laboratory	L-shaped thermosyphon, insulation and crushed-rock revetment	Exp.	Compared traditional methods, significantly enhanced the cooling effectiveness deep within the embankment.
[144]	QTP	Cool foundation	Exp.	Frost jacking observed due to TPCTs, increased tangential frost heaving force.
[145]	Laboratory	Embankment	Exp.	Vapor compression refrigeration system (VCRS) effectively cooled soil below 0 °C with a COP of 0.41.
[146]	Beiluhe Station	Semiconductor refrigeration device	Exp.	TPCT with Semiconductor improved cooling effect, especially during warmer months.
[147]	Fairbanks	Roadway embankments	Exp.	HTPCT reduced temperature discrepancies in embankments by up to 86 %.
[148]	QTP	Four combinations of embankment models	Exp.	Combination of L-shaped TPCT, insulation, and crushed-rock revetment was most effective.
[149]	QTH	Embankment	Exp.	Improved permafrost layer stability; effectiveness varied with positioning and characteristics
[150]	Beiluhe Station	Can be adapted for cooling embankments, airstrip bases, pipe foundations, and other structures	Exp.	Wind-driven thermosyphon device lowered permafrost temperatures by 0.6–1.0 °C, extending cooling impact up to 1.5 m from its placement.
[151]	CRCOP	Ventilation duct	Exp.	U-shaped air U-shaped air ventilation duct (U-AVD) effectively mitigated permafrost thaw around the pipeline, reducing thaw settlement and removing thaw bulb during the cold season.
[152]	QTP	Tower foundations	Exp.	TPCT with vegetation reduced temperature fluctuations of foundation soil, enhanced cooling effect, and provided an environmentally friendly, cost-effective insulation material.
[8]	Not specified	Buried pipeline	Num.	Thermosyphons significantly reduce frost heave and thaw settlement by 62 % and 82 %, respectively.
[9]	Northeast China	Railway embankment	Num.	Reduced freezing depth significantly compared to normal embankments. After ten years, maximum freezing depth was 0.54 m with TPCTs vs. 2.01 m for standard embankments.
[124]	Giant Mine, Canada	Ground freezing applications	Num.	Effective in maintaining permafrost and preventing thawing; optimized with active refrigeration system.
[153]	China	Embankment with combined LTPCT, crushed-rock revetment and insulation	Num.	L-shaped TPCT effective in permafrost regions; enhances cooling performance when combined with crushed-rock revetment and insulation.
[154]	QTR	Embankment in Sandy Permafrost Zone	Num.	TPCTs cool down embankment subbases, reducing ground temperature by more than 1 °C within five years.
[155]	Northeast China	Controlling the soil freezing expansion	Num.	Their findings contributed to understanding the engineering applications of

(continued on next page)

Table 5 (*continued*)

Ref.	Study Location	Applications	Method	Findings
				thermosyphons in cold regions.
[105]	Not specified	Anodized TPCT	Num.	Anodized aluminum thermosyphons revealed significant improvements in heat transfer efficiency, particularly when positioned at specific angles
[166]	Bethel Airport, Alaska	Embankment with thermosyphon	Exp.	The Battle Airport's thermosyphons have considerably lowered subgrade temperatures, strengthening and stabilizing the test area's runway.

can inadvertently induce soil frost heaving. This paradoxical effect, known as frost jacking, results from increased tangential frost heaving force and decreased anti-jacking force, causing the piles to move upward. The study highlighted that artesian groundwater exacerbates this issue by increasing moisture migration. Field observations and computational analysis revealed that the cooling effect of TPCTs around pile foundations significantly heightens the risk of frost jacking, particularly in areas with shallow groundwater. Over a seven-year period, considerable upward movement and differential deformations were observed, leading to potential structural instability. This underscores the need for careful evaluation and maintenance of TPCTs in permafrost regions to prevent such detrimental effects.

Despite the effectiveness of passive thermal barriers and traditional thermosyphons for cooling permafrost, these methods have limitations due to temperature differences and environmental conditions. To overcome these challenges, Hu et al. [145] developed an active refrigeration system using vapor compression technology. They designed a novel vapor compression refrigeration system (VCRS) prototype featuring a coiled evaporator and a piston-type compressor, which was tested in a controlled model environment. The VCRS proved capable of cooling soil below 0 °C, maintaining a refrigerating temperature of −14 °C even when ambient temperatures were positive. This consistent cooling effect extended several meters into the soil, preventing permafrost degradation despite seasonal temperature fluctuations. With an effective coefficient of performance (COP) of around 0.41, the VCRS offers a reliable solution for stabilizing embankments in permafrost regions, maintaining cooling through warm seasons, and mitigating infrastructure impacts due to climate change.

Also, in an effort to address the limitations of traditional vertical thermosyphons, Jin et al. [56] studied a thermosyphon having a horizontally placed evaporator area (HTPCT). This design maintains efficient fluid circulation and heat transfer due to its internal features, such as wicks and return lines. The HTPCT technology specifically targets differential frost heave caused by lateral temperature differences in traditional systems. Field experiments showed that the HTPCT could lower soil temperatures under embankments by up to 1.61 °C more than control sites without cooling, especially during colder periods when its performance was optimal. This more uniform and effective temperature control reduces the risk of embankment cracking and instability, proving superior to traditional cooling systems in managing temperature distributions across embankments. Building on these innovations, Pei et al. [147] conducted a field experiment in Fairbanks, Alaska, to address significant temperature variations along embankment slopes throughout the year. Observing these fluctuations, the team replicated the conditions in a comprehensive laboratory setup to evaluate the efficacy of HTPCT. The experimental setup included a detailed monitoring system to track temperature fluctuations, heat flow, and embankment deformations. The results were impressive: using HTPCT in conjunction with traditional insulation methods reduced temperature discrepancies by up to 86 % compared to setups without HTPCT, demonstrating its significant impact on stabilizing embankment temperatures.

The integration of semiconductor refrigeration devices into a TPCT creates a structure that is simpler, smaller, and operates over a wider temperature range than traditional systems. This innovative approach, explored by Liu et al. [146], was subjected to a comprehensive two-year field test, revealing significant improvements in the cooling effect of the TPCT system. The hybrid system achieved notably lower evaporator temperatures compared to a standard TPCT, resulting in a substantial reduction in ground temperature around the installation. This effect was particularly pronounced during the warmer months, from June to October, when the device's operational peaks occur. The research underscores the hybrid TPCT system's superior heat transfer capabilities, making it more effective than both vapor compression and adsorption refrigeration systems during the warm time.

Extending the investigation of TPCT configurations, Yan et al. [148] performed a set of physical experiments on the QTP. They tested four configurations: inclined TPCT with insulation, inclined TPCT with insulation and crushed rock revetment, L-shaped TPCT with insulation, and L-shaped TPCT with insulation and crushed rock revetment. After seven freeze-thaw cycles, the combination of L-shaped TPCT, insulation, and crushed-rock revetment emerged as the most optimal in maintaining the heat stability of wide-paved embankments. This comprehensive testing demonstrated the robust performance of this configuration in preserving permafrost integrity under varying climatic conditions.

The application of thermosyphons to mitigate permafrost-related damage along the QTH was the focus of Qi et al. [149]. Utilizing ground-penetrating radar to analyze the embankment and permafrost conditions, they found that thermosyphons significantly improved permafrost layer stability compared to areas without such installations. However, the effectiveness of thermosyphons varied based on several factors, including their positioning and the specific characteristics of the permafrost beneath the embankment. This study highlights the nuanced application of thermosyphons and the importance of site-specific considerations in maximizing their efficacy.

To maintain the structural stability of permafrost subgrades, crucial for infrastructure in polar and high-altitude regions, Qin et al. [150] developed an innovative wind-driven device. This device integrates a windmill, a mechanical clutch having phase change medium, and a fluid-circulation heat exchanger, operating by reacting to ambient temperatures: it activates to cool when temperatures drop and shuts off to prevent heat absorption when temperatures rise. Over two years of field testing at the Beiluhe Permafrost Station on the Qinghai-Tibet Plateau (QTP), the device proved effective, lowering permafrost temperatures by 0.6–1.0 °C and consistently extending its cooling impact up to a radius of 1.5 m from its placement. The study underscores the device's versatility, suggesting its potential applications across various types of infrastructure, such as embankments, airstrip bases, and pipeline foundations. Its customizable design allows for adjustments in size and configuration to suit diverse permafrost conditions, making it a flexible solution for maintaining stability in cold regions.

Addressing the challenges of rapid permafrost thaw under the China-Russia Crude Oil Pipeline (CRCOP), Cao et al. [151] introduced a novel technique using a U-shaped air ventilation duct (U-AVD) to mitigate thaw settlement. Employing a comprehensive field monitoring system to gather real-time data on pipeline-permafrost interactions and an indoor model testing platform to evaluate the U-AVD's cooling performance, the study demonstrated the technique's effectiveness. The U-AVD leverages natural cold energy to cool the permafrost during winter. Indoor tests simulating real-world conditions showed that the U-AVD effectively mitigated permafrost thaw around the pipeline, reducing thaw settlement and eliminating the thaw bulb during the cold season. This innovative approach provides a practical solution for managing

permafrost stability in areas affected by infrastructure-related heat.

In another innovative approach, Guo and Zhang [152] explored the use of thermosyphons combined with vegetation cover to improve the stability of transmission tower foundations in permafrost areas on the QTP. Vegetation helps reduce temperature fluctuations at the ground surface, creating a more stable thermal environment for the foundation soils. This additional layer of insulation lowers the average annual ground surface temperature, thereby enhancing the cooling effect of the thermosyphons. Compared to synthetic materials like insulation boards, using vegetation as an insulating material is more environmentally friendly. Additionally, vegetation cover can be a cost-effective alternative to traditional insulating materials, potentially reducing overall construction and maintenance costs while providing effective thermal regulation and restoring and beautifying the landscape. This study highlights the dual benefits of using natural materials in conjunction with thermosyphons: environmental sustainability and improved thermal management.

3.3. Numerical simulations

Numerical simulation helps understanding and optimizing the performance of thermosyphons in cold regions. These simulations allow researchers to predict the thermal nature of thermosyphon structures under various environmental conditions and configurations, providing insights that guide their practical application in infrastructure projects.

For effective TPCT operation, the section exposed to the atmosphere must be cooled below the fluid's temperature at the base of the TPCT. As vapor condenses within the cooler zone, it releases heat and consequently induces a reduction in pressure within the vessel. This pressure decrement initiates boiling in the liquid pool, resulting in evaporation. By the action of gravity, the condensed liquid is channeled from the upper to the bottom end of the TPCT. If this liquid encounters a segment of the vessel surface at a higher temperature during its descent, it re-evaporates. The cycle recommences when the temperature at the TPCT's upper end is some degrees exceeding that at the bottom [154]. This mathematical model draws upon the established principles of TPCTs as detailed by Zhuang and Zhang [28], and Pan and Wu [155], in conjunction with An et al.'s [171] theoretical framework for thermal conduction with phase change in soils. The forthcoming section presents an integrated thermal energy transport model, encapsulating the interplay between air, the TPCT, and soil within the structural confines of a TPCT embankment. Fig. 3 unveils the TPCT's thermal resistance network, systematically identifying the thermal resistances labeled R_1 through R_6. Based on the working approach of TPCT and on the theory of thermal conduction with phase change for soils, a coupled thermal energy transport model of air-TPCT-soil for TPCT embankment is in the following [172].

3.3.1. Thermal model for TPCT

Numerical studies, such as Zhang et al. [172,173], approached the heat transfer in TPCTs by dividing them into three groups: evaporator, adiabatic, and condenser. The total heat resistance for thermal energy transport from the air above the ground to the soils surrounding the evaporator area includes the sum of the heat resistances in the condenser area, the adiabatic area, and the evaporator area (Fig. 3). In the condenser area, the thermal flux encounters three thermal resistances: R_1, which represents the heat resistance between the air and the TPCT's finned outer surface; R_2, which characterizes the heat resistance of the condenser section's tube surface, and R_3, which denotes the heat resistance due to the liquid film within the condenser section. In the adiabatic zone, the heat flux needs to overcome R_4, the heat resistance of the adiabatic zone. R_4 is a step function that describes the thermal resistance depending on the TPCT's operational status. During active phases, when vapor ascends and liquid descends through the adiabatic zone, the heat resistance is significantly reduced. In contrast, when the TPCT is idle and the vapor remains static, the thermal resistance becomes effectively

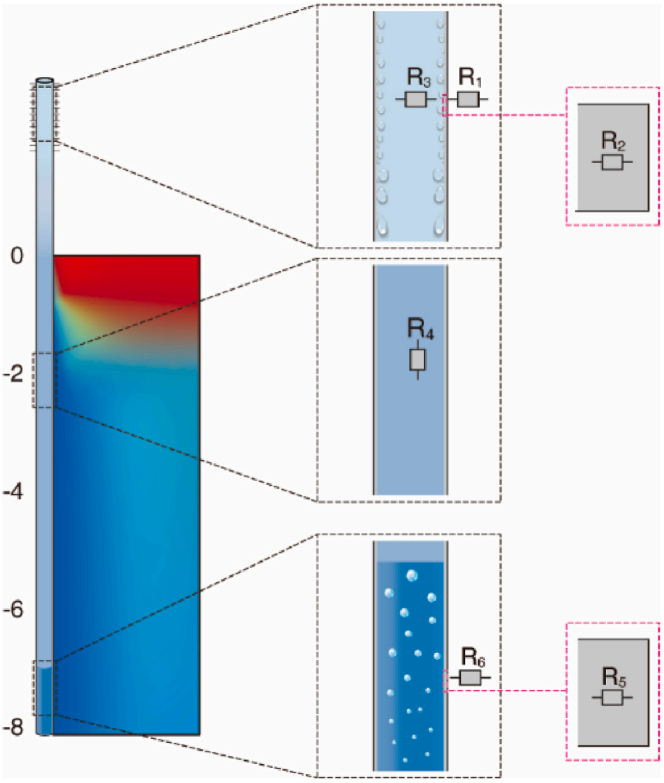

Fig. 3. Thermal Resistance Model of a TPCT, inspired by Ref. [172]. Note: overall heat resistance $R=R_1+R_2+R_3+R_4+R_5+R_6$.

infinite. This step function highlights the conditional nature of the adiabatic section's thermal resistance based on the TPCT's operational state [172]. In the evaporator zone, the thermal flux must overcome the aggregate thermal resistance R_5, which includes the liquid film and the liquid pool components, and the thermal resistance R_6 across the TPCT wall. A schematic representation of these thermal resistances can be found in Fig. 3, and detailed calculations of these thermal resistances are available in Ref. [172].

Summarizing the analysis above, the overall heat resistance of the TPCT is defined as:

$$\sum R_i = R_1 + R_2 + R_3 + R_4 + R_5 + R_6 \tag{1}$$

The entire heat flux, Q (W), traversing through the TPCT, is determined by the cumulative temperature differentials over the individual resistances, formalized by:

$$Q = \frac{T_a - T_s}{\sum R_i} \tag{2}$$

In this context, T_a denotes the average air temperature outside the heat pipe condenser, while T_s indicates the average soil temperature surrounding the heat pipe evaporator. Furthermore, based on the computational analysis that was conducted by Wang et al. [140], the conceptual thermal energy transport model for the TPCTs can be described with the following relation:

$$\begin{cases} Q(F,\alpha,\Delta T,t) = \alpha \times F \times \Delta T(t) \times \eta \ \Delta T > 0.8 \\ Q(F,\alpha,\Delta T,t) = 0 \ \Delta T \le 0.8 \end{cases} \tag{3}$$

Here, F is the thermal exchange area (m^2), ΔT is the temperature drop between the air and the soil around the evaporator zone ($T_a - T_s$), the critical value is usually kept to be 0.8 [174–176]. η is the thermal energy dissipation efficacy of the fins [177]. α (W/($m^{2\cdot}$°C)) is the convective thermal energy transport parameter between the condenser section and the air and expressed as follows:

$$\alpha = \frac{N_{ua}\lambda_a}{d_0} \tag{4}$$

where N_{ua} is the fluid Nusselt number, λ_a is the air heat conductivity, and d_0 is the outside diameter of the TPCT. The thermal flux density for the evaporator zone is defined as:

$$q = \frac{Q}{\pi d_0 l} = \frac{\alpha \times F \times \Delta T(t) \times \eta}{\pi d_0 l} \tag{5}$$

where l is the size of the evaporation zone (in meters). It is hard to find this length, and previous simulations have not taken note of it. If l is the length from the bottom of the fluid pool to its upper level in the hibernate state, deviation occurs. Where the fluid boils and bubbles generate in the working medium, the upper level of the medium rises and the degree of rise depends on the boiling intensity. As a result, there needs to be a critical review of this length. Furthermore, the non-uniform temperature distribution within the evaporator section complicates the determination of a representative temperature for thermal modeling. Typically, the lowest temperatures occur at the liquid surface at the top of the evaporator, where the evaporation cools it the most. Conversely, the bottom of the evaporator, closer to the heat source, experiences higher temperatures due to vigorous convective heat transfer driven by the boiling process. This gradient poses significant challenges in accurately modeling the thermal dynamics of thermosyphons and affects the overall efficiency and design considerations. This detail has not been thoroughly explored in existing literature, particularly in how it impacts the performance and operational efficiency of thermosyphons. Future studies are essential to address this issue, with a focus on empirical and simulation-based investigations to better understand and characterize the temperature profiles within the evaporator sections. Such research will provide critical insights necessary for optimizing thermosyphon design and improving predictive models for their operation under varied thermal loads and environmental conditions.

3.3.2. Thermal model for soil layers

The effectiveness of thermosyphons in permafrost embankments within snowy environments was investigated numerically by Lu et al. [178]. Simulations were conducted for two scenarios: Case 1, which modeled a snow-covered embankment in winter, including slopes and shoulders, and Case 2, which incorporated thermosyphons angled at 70° to the embankment's toe. When modelling the temperature field of embankments in permafrost areas, the apparent thermal capacity technique is employed. This method excludes heat convection and other thermal phenomena, concentrating exclusively on thermal conduction and the phase change between ice and water. Consequently, this allows for a precise representation of the soil temperature field. Additionally, unfrozen water is treated as a temperature-dependent variable in this model. Therefore, the primary determinant of soil temperature variations over time is the thermal conduction equation, which is defined as [140,179,180]:

$$\rho C_s \frac{\partial T}{\partial t} = \frac{\partial}{\partial x}\left(\lambda_x \frac{\partial T}{\partial x}\right) + \frac{\partial}{\partial y}\left(\lambda_y \frac{\partial T}{\partial y}\right) + \frac{\partial}{\partial z}\left(\lambda_z \frac{\partial T}{\partial z}\right) \tag{6}$$

where ρ is density of soil (kg/m^3), and T represents the temperature in degrees Celsius (°C) and is a scalar quantity; However, the temperature gradient (denoted as $\frac{\partial T}{\partial x}$) is a vector field. While t denotes time (s); C_s is specific capacity (J/(kg·°C)) and λ represents the thermal conductivity measured in watts per meter per degree Celsius (W/(m·°C)) of the soil. Because changes in soil temperature around 0 °C lead to the phase transition between ice and water, which significantly affects soil temperature, this phase transition process must be taken into account in the calculations. In numerical simulations, it is assumed that the phase transition occurs only within a specific temperature range. This process can be represented by variations in soil specific heat and thermal conductivity [60]. Researchers have defined the equivalent heat capacity, $C_s(T)$, and equivalent thermal conductivity, $\lambda(T)$, in Equation (6) based on the sensible heat capacity method [171,181]. These are expressed in accordance with the temperature range and the corresponding freezing-thawing state, as [182]:

$$C_s(T) = \begin{cases} C_f & T < T_m - \Delta T \\ \dfrac{C_u + C_f}{2} + \dfrac{L}{2\Delta T} & T_m - \Delta T \le T \le T_m + \Delta T \\ C_u & T > T_m + \Delta T \end{cases} \tag{7}$$

$$\lambda(T) = \begin{cases} \lambda_f & T < T_m - \Delta T \\ \lambda_f + (\lambda_u - \lambda_f)\left[(T - (T_m - \Delta T)\right]/2\Delta T & T_m - \Delta T \le T \le T_m + \Delta T \\ \lambda_u & T > T_m + \Delta T \end{cases} \tag{8}$$

Here, C_f and C_u denote the specific heat capacities (J/(kg·°C)) of frozen and unfrozen soil, respectively. Similarly, λ_f and λ_u represent the heat conductivities in frozen and unfrozen conditions(W/(m·°C)), respectively. T_m is the temperature on the freeze-thaw interface.

In order to calculate the latent thermal energy arising from the phase change between ice and water within soil pores, the following expression can be used instead of Eq. (6) [140,183]:

$$\rho C_s(T)\frac{\partial T}{\partial t} = \frac{\partial}{\partial x}\left(\lambda(T)\frac{\partial T}{\partial x}\right) + \frac{\partial}{\partial y}\left(\lambda(T)\frac{\partial T}{\partial y}\right) + \frac{\partial}{\partial z}\left(\lambda(T)\frac{\partial T}{\partial z}\right) + L\rho_i\frac{\partial \theta_i}{\partial t} \tag{9}$$

where ρ_i is refers to density of ice, L represents the latent thermal energy involved in the ice phase change which equals 335 kJ/kg [183], and θ and θ_i indicate the volumetric moisture and ice contents, respectively. Tai et al. [184] estimate ice's latent heat term as follows:

$$L\rho_i\frac{\partial \theta_i}{\partial t} = L\rho_i\frac{\partial(\beta_i\theta_u)}{\partial t} \approx L\rho_i\frac{\partial \beta_i}{\partial t}\left[(\theta_s - \theta_r)S_r + \theta_r\right] \tag{10}$$

where θ_u, θ_s, and θ_r, represent the volumetric unfrozen moisture content, saturated moisture content, and residual moisture content of the soil, respectively. S_r denotes the relative degree of saturation of frozen soil. β_i is defined as the ratio of ice content to unfrozen moisture content in volume terms [183]:

$$\beta_i = \frac{\theta_i}{\theta_u} \tag{11}$$

The interaction involving the thermal energy transport between the TPCT and the soil manifests through a thermal balance equation, which is formalized as follows [185]:

$$\frac{T_a - T_s}{\pi d_o l \sum R_i} = -\lambda_s \frac{\partial T}{\partial n} \tag{12}$$

where l represents length of evaporation section; $\frac{\partial T}{\partial n}$ stands for temperature gradient in the direction normal (perpendicular) to the outer skin of the thermosyphon.

3.3.3. Boundary conditions

The thermodynamic approach for TPCT embankments, characterized by its high nonlinearity, necessitates solutions using numerical methods. Details on the solution procedure and the computational techniques of the coupled thermodynamic approach are available in Ref. [186]. Simulating the heat performance of the thermosyphon requires defining the boundary in the computation domain. At a soil profile far away from the thermosyphon, where the border is set as adiabatic. At the border of the computation domain, which is usually 10–20m lower the natural ground, the natural ground temperature gradient of 0.03 °C/m is usually specified. Usually, at the natural ground or the embankment surface of the side slope surface, a sinusoidal temperature boundary is considered as follows:

$$T = A\sin(wt_h + B) + C \tag{13}$$

In which A is the amplitude, B is the phase, and C is the annual mean surface temperature. There are many studies that arbitrarily specify these parameters [187]. C and A values for various borders are listed in Table 6.

It is interpretable that this sinusoidal temperature wave can be specified for the natural ground and the side slope or the embankment because such specification reduces the computational time. However, this problem is that if $T = A\sin(wt_h + B) + C$ is specified for the air, the thermosyphon would keep working for an entire day during the winter time and keep idling on an entire day in summer time. This is not true because even in winter, the thermosyphon works intermittently because the air temperature rises during the daytime, especially around solar noon. This rise in air temperature at noon time makes the thermosyphon hibernate. In summer time, the thermosyphon can occasionally work at midnight and idle at noon. Therefore, the thermosyphon always shifts from working to idling repeating. This cannot be captured in the current simulations. Intuitively, such intermittent heat transfer can more effectively drain the heat of the soils. If this is true, the cooling efficiency of the thermosyphon may be underestimated in the current numerical model.

The four lateral surfaces are treated as adiabatic. Additionally, the wind velocity at a height H meters above the ground surface can be modeled as follows [190]:

$$v_H = v_{10}\left(\frac{H}{10}\right)^{0.16} \tag{14}$$

where v_{10} is the wind velocity at 10 m over the ground. Long-term meteorological data provides the following formulation for v_{10} [190]:

$$v_{10} = 3.64 + 1.10\sin\left(\frac{2\pi}{8760}t_h + \frac{3}{2}\pi + \alpha v_0\right) \tag{15}$$

Table 6
Temperature boundary characteristics for various surfaces.

Surface type	Location	Ref.	C (°C)	A (°C)
Ambient air	QTR	[134]	−3.5	14
	QTP	[172,188]	−3.5	11.5
	QTR	[173]	−4	11.5
	Highways	[148]	−3.69	–
	West China	[153]	−4	11.5
	QTP	[154]	−5.5	12
	QTP	[180]	−3.82	11.5
	Mohe	[178]	−4.37	23.42
Natural ground surface	QTR	[134]	−1	10
	QTP	[172,186]	−0.5	12
	QTR	[173]	−1.5	12
	Highways	[148]	−1.88	–
	QTP	[60]	−1	11.5
	QTP	[154]	−1	12
	QTP	[180]	−1.32	12
	Mohe	[178]	0.03	15.99
	West China	[153]	−1.5	12
	Changchun	[9,189]	2.5	19.9
Soil slope	QTR	[134]	0.5	12
	QTP	[186]	0.7	13
	Highways	[148]	0.94	–
	QTP	[60]	0.3	12
	QTP	[180]	−2.26	15.5
	Mohe	[178]	1.9	17.56
	West China	[153]	0.7	13
Not specified	Changchun	[9,189]	3.5	21.9
Asphalt pavement	QTR	[134]	0.5	14
	QTR	[186]	1.5	15
	Highways	[148]	3.23	–
	QTP	[60]	5.3	15.6
	QTP	[180]	2.88	15
	Mohe	[178]	1.39	24.88
	West China	[153]	2.5	15

3.3.4. Freezing and thawing indexes

In regions characterized by permafrost, the environmental conditions, specifically the freezing and thawing cycles, significantly impact the operational efficiency of TPCTs [191]. To understand and predict these effects, it is essential to consider the freezing and thawing indexes, which provide a quantitative measure of the climatic conditions relevant to TPCT applications [140]. The Freezing Index is a cumulative measure of all daily mean temperatures below 0 °C during the designated freezing period of a year [192]. Mathematically, it is expressed as [193]:

$$FI = \sum_{i=1}^{N_F} |T_{a\_i}|, T_{a\_i} < 0 \tag{16}$$

where T_{a_i} represents the daily mean temperature of the air, and N_F is the number of days with temperatures below freezing.

Conversely, the Thawing Index sums all daily mean temperatures above 0 °C during the thawing period [193]:

$$TI = \sum_{i=1}^{N_T} |T_{a\_i}|, T_{a\_i} > 0 \tag{17}$$

where N_T is the number of days with temperatures above zero. These indices are pivotal for assessing the thermal dynamics in permafrost areas, impacting the design and function of TPCTs. Frost Number provides a dimensionless measure that incorporates both the freezing and thawing Indices to assess freeze-thaw conditions [140]:

$$FN = \frac{FI}{TI} \tag{18}$$

This formula offers a more nuanced view of the thermal dynamics within permafrost regions by emphasizing the relative intensities of freezing and thawing processes [194]. A Frost Number greater than 1 indicates that the freezing capacity of the climate exceeds the thawing capacity, leading to potential soil freezing trends. Conversely, a Frost Number less than 1 suggests a greater thawing capacity, possibly indicating rapid permafrost degradation. An FN equal to 1 signifies an equilibrium state where freezing capacity matches thawing capacity, often leading to unstable soil conditions. TPCTs need to be adapted and designed considering these Frost Number variations to ensure they are effective in their specific deployment environments. Adjustments in design might include changes in the working fluid, adjustments in system dimensions, or alterations in installation patterns to optimize their performance according to local climatic conditions.

3.3.5. Simulation cases

Wen et al. [134] conducted a comprehensive investigation into four embankment configurations at altitudes exceeding 4000 m: a common embankment, an embankment having insulation, an embankment with thermosyphons, and one with both insulation and thermosyphons. Utilizing 3D computational approach, the study simulated the heat behavior of these configurations over 50 years. The boundary conditions in their model considered a variety of factors including the initial temperature patterns received through long-term transient solutions, the physical parameters of the soil, and a projected rise of air temperature of 2.0 °C over the next 50 years. The ground surface temperature was adjusted for radiation effects, making it 2.5 °C higher than the annual average air temperature, and specific heat flux values were assigned to the boundaries. The findings revealed that combining insulation with thermosyphons is the most effective strategy for protecting permafrost, ensuring long-term stability and thermal control in warming climates.

Li et al. [180] studied a sophisticated thermodynamic approach formed on conservation principles to analyze the seismic responses of embankments over different seasons following a decade of operational analysis. Their simulations assessed the embankments' responses to seismic activity across four distinct seasons, using the variability in seasonal heat regimes and their influence on the mechanical behaviour of the embankments. TPCT embankments demonstrate diverse thermal performances depending on the season. Given that soil exhibits strong

nonlinearity and the thermomechanical behaviour of frozen soil is temperature-dependent, the dynamic model was formulated using incremental equations. This model adheres to models of mechanical equilibrium, continuous deformation, mass conservation, and the stress-strain relationship [186,195].

Tian et al. [183] conducted a study involving the continuous monitoring of two highway embankment sections over three years: a conventional embankment and an embankment with thermosyphons mounted on the sunny slope surface. They recorded ground temperature and settlement at various depths. Additionally, a coupled hydro-thermal-mechanical approach was employed to simulate and predict the performance of different thermosyphon configurations over a 30-year period under climate warming scenarios. The model simulations indicated that installing thermosyphons on both surfaces of the embankment provides the most effective performance. Their numerical setup included a thaw settlement model, where the overall settlement of the permafrost was comprised of settlement owing to phase transition and consolidation under self-weight and external load. The thaw settlement was estimated using the following formula:

$$S = A_0 h_0 + \alpha_0 hP \tag{19}$$

where A_0 is the permafrost thaw settlement parameter, h_0 is the permafrost thickness, α_0 is the compressibility parameter of thawed permafrost, h is the thawed ground thickness, and P is the overburden pressure.

Using the finite element software ABAQUS, Park et al. [8] delved into the role of thermosyphons in reducing frost heave and thaw settlement in pipelines buried in frost-sensitive soils. The soil, modeled as frost-susceptible and prone to volume changes from freezing and thawing, had its mechanical and thermal properties calibrated with experimental data. The pipeline, represented as an elastic structure within the frost-susceptible soil, showcased the interaction between the soil and pipeline. Remarkably, the study revealed that thermosyphon arrangement could reduce frost heave and thaw settlement by up to 62 % and 82 % respectively, compared to scenarios without thermosyphons. Chen et al. [154] advanced the understanding by creating a comprehensive numerical model to simulate heat exchange among thermosyphon, air, and soil layers. This model included air convection through a crushed-rock interlayer, heat conduction with phase changes, and the coupled air-TPCT-soil system. The outcomes were striking that TPCTs effectively cooled embankment subbases and subgrades, reducing ground temperature by over 1 °C within five years. The timing of TPCT installation played a crucial role; installations in the 10th year of operation notably mitigated warming and sand accumulation effects, while installations in the 30th year offered a more limited cooling range, underscoring the importance of early intervention.

Gao et al. [9] focused on the heat impacts of heating two-phase closed thermosyphons on high-speed railway embankments in seasonally frozen areas. Their innovative approach combined solar and electric heating to warm subgrade layers beneath a concrete track plate. 3D thermal energy transport approach simulated the thermal characteristics of embankments with TPCTs over a decade, incorporating heat and mass transfer principles. TPCTs automatically switched to electric heating when temperatures fell below freezing. The study showed a dramatic reduction in freezing depth with TPCTs; after ten years, the maximum freezing depth beneath the track plate was 0.54 m, compared to 2.01 m in a standard embankment.

Pei et al. [153,196] constructed an intricate three-dimensional heat transfer model to simulate convective, conductive, and phase-change heat transfer mechanisms. This model integrated L-shaped TPCTs within an embankment topped with heat-absorbing asphalt pavement, typical of high-grade highways in permafrost regions. The model considered the heat resistance of various TPCT sections and their interaction with surrounding soil. Additional cooling measures included crushed-rock revetment and an insulation layer. The simulations evaluated crucial metrics like permafrost thaw depth, temperature distribution, and overall thermal stability. Findings revealed that the optimal arrangement combined LTPCTs with crushed-rock revetment and insulation, effectively cooling the permafrost, particularly in the initial years post-construction. This setup efficiently managed thermal exchange, decreasing thermal absorption in warm months and utilizing ambient energy in cold periods.

While the majority of simulations assume that thermosyphons are positioned on the Qinghai-Tibet Plateau or other locations within China, some studies have investigated the heat performance of thermosyphons situated outside of China. Zueter and Newman [124] conducted a numerical study on hybrid thermosyphons, focusing on their application at the Giant Mine in Canada. This research highlighted the efficiency of hybrid thermosyphons in maintaining permafrost and preventing thaw-induced environmental hazards. Operating in passive mode during cold seasons and active mode with a refrigeration system in warm seasons, hybrid thermosyphons ensured year-round stability. Their numerical setup, was based on the mentioned equations including heat resistance network approach coupled with a transient two-phase heat conduction equation (Eq. (17)). For validation of their setup, they used the lab and field data from the Giant Mine. Furthermore, they explored design and operational parameters to optimize hybrid thermosyphon efficiency, finding that lower coolant temperatures and higher flow rates enhanced freezing, though excessively low temperatures led to unnecessary energy consumption. The study provided valuable insights for optimizing hybrid thermosyphon systems for effective permafrost protection and energy efficiency.

The numerical simulations discussed, along with other unreported studies, share a common issue: validation is seldom addressed. This lack of validation is partly due to the technical challenges involved and, in some cases, the impossibility of achieving it. Numerous uncertain parameters influence the simulations, including soil properties, geometric boundaries of the model, thermal flux boundaries, and the calculation of the thermosyphon's thermal flux. Typically, the soil beneath the surface is assumed to be layered, with uncertain composition and moisture content. The geometric boundary in simulations should ideally be three-dimensional, given that the thermosyphon radiates cooling from its center, and the surrounding boundary is not uniform. The heat flux boundary is often assumed to be a Dirichlet boundary, with sinusoidal temperature waves imposed on the top boundary with the side slope, natural ground, and other exposed surfaces. The amplitude and mean of these temperature waves are specified empirically and somewhat arbitrarily. Using this sinusoidal temperature to calculate the thermosyphon's operating and idle hours makes it difficult to accurately predict the cooling process. Most critically, the calculated thermal resistances of the thermosyphon are often not validated. Therefore, while numerical simulations can demonstrate cooling trends of thermosyphons in permafrost regions, the accuracy of the cooling magnitude and distribution remains uncertain.

4. Future perspectives

4.1. Material advancements and durability of thermosyphon

The efficiency and durability of thermosyphons, particularly in the demanding environments of cold regions, are heavily influenced by the materials from which they are constructed [197]. Innovations in material science have led to significant improvements in these aspects, enabling thermosyphons to operate more effectively and withstand the rigors of extreme conditions. The traditional materials for thermosyphon construction include copper, aluminum, and stainless steel, known for their good thermal conductivity and corrosion resistance. However, the quest for improved performance and durability, especially under extreme cold conditions, has driven the exploration of advanced metals and alloys. For instance, nickel-based alloys and titanium have gained attention for their exceptional strength and resistance to

low-temperature brittleness, making them ideal for applications in sub-zero environments [198,199]. These materials not only ensure the structural integrity of thermosyphons but also enhance their thermal performance by maintaining optimal heat transfer capabilities in cold climates.

The durability of thermosyphons can be significantly influenced by local geological conditions and the corrosive nature of different soils [133,200]. The presence of aggressive ions, such as chlorides and sulfates in soil, can accelerate corrosion in less resistant materials [201]. It is crucial to choose materials based on specific soil chemistries where the thermosyphon will be installed. Acidic or highly alkaline soils can also degrade certain materials faster than neutral soils [202]. Applying protective coatings such as epoxy or zinc plating can significantly enhance the corrosion resistance of traditional materials like steel and aluminum [203]. Composite materials, combining two or more constituent materials with contrasting properties, have emerged as a promising option for thermosyphon construction. The strategic integration of composites can offer a balance of lightweight, high strength, and superior thermal insulation properties, making them ideal for the adiabatic section of thermosyphons. For example, carbon fiber-reinforced polymers (CFRPs) are being explored for their potential to reduce the overall weight of thermosyphons while maintaining high tensile strength and reducing thermal bridging [204–206], thereby enhancing the efficiency of heat transfer in cold environments.

Developing hybrid materials that combine the mechanical strength of metals with the corrosion resistance of ceramics or polymers can provide tailored solutions that address the specific needs of different permafrost regions. There is a need for more comprehensive regional studies that evaluate the performance of various thermosyphon materials under local soil conditions [207]. Such studies would help in developing region-specific material guidelines and installation practices. Ongoing research into nano-enhanced materials and bio-inspired coatings could further improve the durability and efficiency of thermosyphons in corrosive environments.

4.2. Cost-effectiveness. Of thermosyphons

While thermosyphons effectively reduce permafrost temperatures and adapt to climate change impacts, their economic feasibility remains a significant concern due to the high initial investment and ongoing maintenance costs [208]. Thermosyphons, though highly effective in stabilizing permafrost, come with considerable initial costs [209]. These costs are primarily driven by the need for durable materials and sophisticated engineering designs to withstand harsh environmental conditions. The installation process, which often involves deep drilling and specialized equipment, further adds to the expense. Moreover, the effective area of thermosyphons is relatively small—typically only a few meters—which means that numerous units may be required to cover the necessary area, multiplying the initial investment [208].

Maintenance costs can also be significant, especially in remote or inaccessible areas where routine inspections and repairs become logistically challenging and expensive [210]. The annual cost for maintaining, repairing, and preventing pipeline deformation due to changes in permafrost conditions is estimated at $1.5 billion [211]. These factors must be meticulously evaluated against the projected lifespan and the potential cost savings in terms of reduced repair and maintenance of the protected infrastructure.

To improve the cost-effectiveness of thermosyphons, ongoing research and development efforts are concentrating on optimizing their designs and materials [212]. The goal is to extend their functional lifespan and minimize maintenance frequency and costs. Innovations in materials, such as advanced composites or corrosion-resistant alloys, may have higher initial costs, but they can significantly reduce lifecycle expenses by enhancing durability and performance in extreme conditions. Despite the high upfront costs, the long-term benefits of using thermosyphons can justify the investment. By effectively maintaining the integrity of infrastructure, thermosyphons reduce the need for costly repairs and replacements that would be necessary as permafrost thaws due to climate change. Economic models that include cost-benefit analyses, taking into account the extended lifespan of infrastructure and the prevention of costly failures, often show a positive return on investment over the long term [213].

Detailed case studies of projects incorporating thermosyphons can provide insightful data on cost-effectiveness [214]. For instance, the use of thermosyphons in the Trans-Alaska Pipeline System has demonstrated how effective these systems can be in preserving the structural integrity of large-scale infrastructures in permafrost regions [6]. Comparative analyses with other cooling and stabilization technologies can also highlight the conditions under which thermosyphons present a more economically viable option.

Further research into cost-reduction strategies is essential. This could include the development of modular or adjustable thermosyphons that can be easily installed and maintained or the integration of thermosyphons with renewable energy sources to reduce operational costs [215].

4.3. Surface area enhancements: maximizing heat transfer capability

Nanoparticle coatings significantly enhance thermosyphon performance by increasing surface area and improving heat transfer characteristics, which is particularly beneficial in cold climates. These surface treatments and advanced coatings improve the durability and efficiency of thermosyphons by enhancing resistance to corrosion, icing, and mechanical wear, thus extending their operational lifespan in harsh environments. Hydrophobic or icephobic coatings, for example, prevent ice accumulation on external surfaces, maintaining consistent performance under cold conditions.

Recent advancements in thermosyphon technology include optimizing the boiling process through surface modifications that increase the surface area. Solomon et al. [105] demonstrated a 15 % increase in heat transfer coefficient (HTC) using an anodized aluminum thermosyphon with nanopore structures, compared to a non-anodized counterpart. This study highlighted that positioning the thermosyphon at a 45° angle could enhance the evaporator's HTC by up to 33 %, whereas a 90° inclination reduced overall thermal resistance by 23 %.

Further research by Hsu et al. [216] on the application of nanoparticle silicate coatings within the evaporator and condenser zones found that such coatings created superhydrophilic and superhydrophobic surfaces, reducing thermal resistance by 26.1 %. Additionally, Weng and Yang [217] observed that a growth of the length and diameter of an anodized aluminum alloy thermosyphon reduced heat resistance by 58.68 % and delayed dry out by 40 %. Rahimi et al. [218] coated thermosyphon's sections with nanocavity particles, resulting in a decrease in thermal resistance by more than twofold and a 15.27 % improvement in thermal efficiency. These findings underscore the potential of nanoparticle coatings and anodization in enhancing the heat performance of thermosyphons across a variety of operational characteristics.

4.4. Design enhancements

Chen et al. [60] and Jin et al. [56] explored ways to improve the stability of expressway embankments in permafrost areas, addressing the tendency of these structures to deform and crack over time. Their research revealed the drawbacks of traditional inclined thermosyphons, which can lead to uneven soil temperatures and accelerated permafrost thaw. Their extensive numerical modeling demonstrated the superior performance of horizontal thermosyphons, which consistently lower base temperatures across embankments, thereby improving thermal stability. This research introduced an innovative design, the Horizontal TPCT, which incorporates a horizontally embedded evaporator section within the embankment. This design is tailored to address differential frost heave and prevent cracking, offering a viable solution for

constructing expressways in permafrost zones.

Further developments in thermosyphon technology have been pursued in Russia since 1993, focusing on creating small-diameter devices for thermally stabilizing soils around piles [11]. Recent advancements have also included the integration of thermoelectric modules to create active cooling systems within thermosyphons, although this approach is constrained by the cooling capacity and the practical challenges of powering devices in remote permafrost areas. These findings highlight the ongoing need for innovative solutions in thermosyphon design to enhance their effectiveness in permafrost cooling applications.

4.5. Low GWP refrigerants

In the field of thermosyphons, the selection of working fluids warrants a critical examination of their environmental impacts, particularly their global warming potential (GWP) [219]. Historically, fluorinated gases (F-gases) such as R134a and R410A have been the preferred working fluids in two-phase thermosyphon systems within data centers due to their effective thermophysical properties despite their high GWP [220]. This environmental burden is driving a shift towards more sustainable alternatives.

Recent trends in sustainable technology advocate for the adoption of low GWP refrigerants to lessen ecological risks. Notably, hydrofluoroolefins (HFOs) such as R1234yf and R1234ze have emerged as promising substitutes, offering GWPs of less than 1 and 7, respectively [221–223]. These refrigerants present a significantly reduced environmental impact while maintaining performance comparable to traditional hydrofluorocarbons (HFCs). Specifically, R1234yf [224,225], and R1234ze(E) [226] are increasingly considered viable replacements for high-GWP HFCs like R134a.

Moreover, hydrocarbon refrigerants such as R600a (isobutane) offer an environmentally friendly alternative due to their zero ozone depletion potential (ODP), low GWP, low toxicity, and cost-effectiveness [227–229]. R600a aligns well with the EU F-gas regulations, making it a viable option within this regulatory framework [230]. Additionally, propane (R290), with an ODP of 0 and a GWP of 3, provides operational pressures comparable to R134a, further reinforcing its suitability as an eco-friendly working fluid [231,232].

While numerous studies have examined the energy performance of various working fluids in thermosyphon systems, most research has concentrated primarily on the thermal performance aspect. There remains a gap in comprehensive studies that assess the environmental impacts of these newer, low-GWP refrigerants. Future research should extend beyond theoretical analyses to include experimental investigations on the environmental benefits of using low GWP and ODP refrigerants [233]. This includes detailed studies on the boiling heat transfer coefficients and the potential enhancement of these properties through the integration of nanoparticles in refrigerants such as R600a, R290, R1234yf, and R1234ze. Such studies are crucial for validating the environmental and operational viability of these alternative refrigerants in thermosyphon systems.

4.6. Monitoring the working performance of thermosyphons

Millions of thermosyphons are installed in permafrost regions, serving critical roles in preserving permafrost beneath infrastructure and mitigating freezing heave damage in pavement subgrades. Given the harsh local climates, routine maintenance and monitoring of these thermosyphons are often costly and sometimes unfeasible. Consequently, the operational status of these thermosyphons frequently remains uncertain. A particular concern is the integrity of the thermosyphon's seal, as the internal gas pressure is several times higher than atmospheric pressure. Even minor structural failures, such as small gaps or cracks, can lead to the leakage and eventual depletion of the working fluid due to evaporation.

This potential for progressive erosion underscores the need for innovative monitoring solutions to ensure that the evaporative gas of the working medium condenses and circulates as intended within the thermosyphon. Xie and Guo [234] proposed a novel method to determine if a thermosyphon in the field is operational. They discovered that regardless of whether a thermosyphon is working, the temperature at the condenser section is higher at the top and lower at the bottom, following a linear decrease. Using this correlation, the regression of the outer skin temperature of the condenser section against height yields an intercept in the regression plot. In a specific region, this intercept remains consistent. During the nighttime of a cold season, when the thermosyphon is operational, the outer skin temperature can be measured using infrared thermal imaging or other temperature measurement methods. If the intercept of the outer skin temperature versus height for a series of working thermosyphons is the same, but 1–2 thermosyphons show a significantly different intercept, it can be inferred that these 1–2 thermosyphons are not functioning properly and need to be remedied. This method was first reported in Chinese and later presented at the Eighth International Symposium on Permafrost Engineering [235,236].

According to Xie's method [234], if all thermosyphons in a specific field are either all working or all not working, it is difficult to determine their operational status. Additionally, measurements are limited to the nighttime of cold seasons because the thermosyphons are active during this time, making it costly due to the harsh weather in permafrost regions. Since this method was proposed, there have been few further reports on technology to detect if a thermosyphon is working or not during the times it should be operational. Ideally, thermosyphons should be detected around noon during the warm season. It would be preferable if a monitoring device could assess the vigor of the gas vapor circulation, providing critical data on the thermosyphon's functional status. Remote monitoring capabilities would be particularly advantageous, enabling timely interventions for thermosyphon maintenance or fluid replenishment, thus ensuring their continued effective operation in challenging environments.

5. Conclusions

This comprehensive review has highlighted the crucial role of thermosyphons in thermal management, particularly within permafrost regions. Leveraging natural convection and phase change mechanisms, thermosyphons offer an efficient, passive solution for heat transfer, essential for maintaining the structural integrity of infrastructure in cold climates. Their applications span various fields, including transportation, telecommunications, and energy sectors, underscoring their versatility and indispensability. Notably, two-phase closed thermosyphons have been widely employed to preserve the permafrost subgrade of buildings, railways, highways, transmission tower foundations, and pipeline foundations in North America, Russia, China, and elsewhere.

Significant advancements have been made in the design and implementation of thermosyphons, such as the development of closed-loop systems and the integration of nanorefrigerants. These innovations have enhanced the efficiency and reliability of thermosyphons, making them more effective in mitigating the effects of permafrost thaw and ensuring the longevity of critical infrastructure. Experimental studies and field applications have demonstrated the effectiveness of various thermosyphon configurations, such as L-shaped and horizontal thermosyphons, in stabilizing permafrost. These configurations have significantly reduced ground temperatures and maintained the permafrost table, preventing thaw-induced settlement and structural damage. However, installing thermosyphons with other passive cooling methods to preserve permafrost subgrade can be costly in construction, a challenge that is seldom addressed in the literature. Most of these innovative designs remain conceptual, experimental, or the subject of numerical studies. The cooling performance of a thermosyphon is governed by summing the thermal resistances from the outer air to the inner soil surrounding the evaporator section. Numerical simulations of

thermosyphons in permafrost regions face significant challenges in validation due to uncertain parameters and assumptions, making the accuracy of the cooling magnitude and radiation questionable. Despite their usefulness in showing cooling trends, the precise impact of thermosyphons remains difficult to determine.

Despite these advancements and challenges, thermosyphon performance under varying environmental conditions is stilled need optimized. Future research should focus on refining the design and placement of thermosyphons, exploring new materials and working fluids, and developing monitoring systems to assess their long-term efficacy and durability. Continued research and technological innovation will be essential in enhancing their performance and expanding their applications, thereby contributing to the sustainable development of infrastructure in permafrost areas.

Declaration of competing interest

The authors clarify that there is no conflict of interest for report.

Acknowledgements

This research of Mikhail Sheremet and Mohammad Ghalambaz was supported by the Tomsk State University Development Programme (Priority-2030). This project is also supported by the Basic Research Ability Improvement Project of Young and Middle-aged Teachers in Universities of Guangxi (2022KY0161 and 2023KY0178) and by Guangxi Science and Technology Major Program (GUIKE AB22080073).

Data availability

Data will be made available on request.

References

[1] Hu T-f, Yue Z-r. Potential applications of solar refrigeration systems for permafrost cooling in embankment engineering. Case Stud Therm Eng 2021;26.
[2] Li X, Wu Q, Jin H. Mitigation strategies and measures for frost heave hazards of chilled gas pipeline in permafrost regions: a review. Transport Geotech 2022;36:100786.
[3] Wu Q, Ma W, Lai Y, Cheng G. Permafrost degradation threatening the Qinghai–xizang railway. Engineering 2024. https://doi.org/10.1016/j.eng.2024.01.023.
[4] Li G, Jing H, Volkov N, Ma W, Chen P. Centrifuge model test on performance of thermosyphon cooled sandbags stabilizing warm oil pipeline buried in permafrost. Sciences in Cold and Arid Regions 2021;13:234–55.
[5] Greg" Kinney DG, Roberts D. Slipstream heat addition on the Trans-Alaska pipeline: thermal risk mitigation strategies and lessons learned. Cold regions engineering 2024: sustainable and resilient engineering solutions for changing cold regions. p. 161-173.
[6] Yarmak E. Permafrost foundations thermally stabilized using thermosyphons. OTC arctic technology conference. OTC; 2015. OTC-25500-MS.
[7] Andersland OB, Ladanyi B. Frozen ground engineering. John Wiley & Sons; 2003.
[8] Park D-S, Shin M-B, Park W-J, Seo Y-K. Numerical analysis of frost heave and thaw settlement for pipeline buried in frost-susceptible soil via thermosiphons. Appl Sci 2023;13:1948.
[9] Gao J, Lai Y, Zhang M, Chang D. The thermal effect of heating two-phase closed thermosyphons on the high-speed railway embankment in seasonally frozen regions. Appl Therm Eng 2018;141:948–57.
[10] Zhou Y, Wang X, Niu F, He F, Guo C, Liu D, Jiang D. Frost jacking characteristics of transmission tower pile foundations with and without thermosyphons in permafrost regions of Qinghai–Tibet plateau. J Cold Reg Eng 2021;35:04021004.
[11] Lyazgin A, Bayasan R, Chisnik S, Cheverev V, Pustovoit G. Stabilization of pile foundations subjected to frost heave and in thawing permafrost. Proceedings of the 8th international conference on permafrost. Zurich; 2003. p. 21–5. Switzerland.
[12] Olga T. Reduction in tangential frost heaving forces by the pile geometry change. Archit Eng 2017;2:61–8.
[13] Li H, Lai Y, Wang L, Yang X, Jiang N, Li L, et al. Review of the state of the art: interactions between a buried pipeline and frozen soil. Cold Reg Sci Technol 2019;157:171–86.
[14] Konrad J-M, Morgenstern NR. A mechanistic theory of ice lens formation in fine-grained soils. Can Geotech J 1980;17:473–86.
[15] Lytton R, Pufahl D, Michalak C, Liang H, Dempsey B. An integrated model of the climatic effects on pavements. 1993.
[16] O'Neill K. Numerical solutions for a rigid-ice model of secondary frost heave: US army corps of engineers, cold regions research & engineering laboratory. 1982.
[17] Sheng D. Thermodynamics of freezing soils: theory and application: luleå tekniska universitet. 1994.
[18] Hartikainen J, Mikkola M. General thermomechanical model of freezing soil with numerical applications. Ground freezing 97; frost action in soils. Balkema; 1997. p. 101–5.
[19] Michalowski RL. A constitutive model of saturated soils for frost heave simulations. Cold Reg Sci Technol 1993;22:47–63.
[20] Selvadurai A, Hu J, Konuk I. Computational modelling of frost heave induced soil–pipeline interaction: II. Modelling of experiments at the Caen test facility. Cold Reg Sci Technol 1999;29:229–57.
[21] Ming F, Yu Q-h, Li D-q. Investigation of embankment deformation mechanisms in permafrost regions. Transport Geotech 2018;16:21–8.
[22] Dallimore SR. Observations and predictions of frost heave around a chilled pipeline. Carleton University; 1985.
[23] Park D-S, Shin M-B, Seo Y-K. Frost heave of frost susceptible soil according to performance of thermo-syphon. J Kor Geotech Soc 2021;37:27–40.
[24] Cheng G, Wu Q, Ma W. Innovative designs of permafrost roadbed for the Qinghai-Tibet Railway. Sci China E 2009;52:530–8.
[25] Ding T, Chen X, Cao H, He Z, Wang J, Li Z. Principles of loop thermosyphon and its application in data center cooling systems: a review. Renew Sustain Energy Rev 2021;150.
[26] Singh R, Mochizuki M, Mashiko K, Nguyen T. Heat pipe based cold energy storage systems for datacenter energy conservation. Energy 2011;36:2802–11.
[27] Yu F, Qi J, Zhang M, Lai Y, Yao X, Liu Y, Wu G. Cooling performance of two-phase closed thermosyphons installed at a highway embankment in permafrost regions. Appl Therm Eng 2016;98:220–7.
[28] Zhuang J, Zhang H. Heat pipe technology and engineering application. J Energy Res Util 2000:5–41.
[29] Hassanpour A, Borji M, Ziapour BM, Kazemi A. Performance analysis of a cascade PCM heat exchanger and two-phase closed thermosiphon: a case study of geothermal district heating system. Sustain Energy Technol Assessments 2020;40:100755.
[30] Yue C, Zhang Q, Zhai Z, Ling L. CFD simulation on the heat transfer and flow characteristics of a microchannel separate heat pipe under different filling ratios. Appl Therm Eng 2018;139:25–34.
[31] Kuang Y, Yi C, Wang W. Modeling and simulation of large-scale separated heat pipe with low heat flux for spent fuel pool cooling. Appl Therm Eng 2019;147:747–55.
[32] Zhang P, Wang B, Shi W, Li X. Experimental investigation on two-phase thermosyphon loop with partially liquid-filled downcomer. Appl Energy 2015;160:10–7.
[33] de Haan V-O, Gommers R, Rowe JM. Thermodynamic calculations of a two-phase thermosyphon loop for cold neutron sources. Cryogenics 2017;85:30–43.
[34] Cao J, Chen C, Su Y, Leung MKH, Bottarelli M, Pei G. Experimental study on the temperature management behaviours of a controllable loop thermosyphon. Energy Convers Manag 2019;195:436–46.
[35] Cao H, Ding T, He Z, Li Z. Research on the refrigerant column height in the downcomer of a two-phase loop thermosyphon. Int J Refrig 2018;94:40–8.
[36] Ghaffari O, Al Sayed C, Vincent M, Larimi YN, Grenier F, Jasmin S, et al. Two-phase closed-loop thermosyphon filled with a dielectric liquid for electronics cooling applications. 2021 20th IEEE intersociety conference on thermal and thermomechanical phenomena in electronic systems (iTherm). IEEE; 2021. p. 74–80.
[37] Birajdar MR, Sewatkar C. Numerical analysis of closed loop thermosyphon system used to cool the electronic devices. Conference on fluid mechanics and fluid power. Springer; 2021. p. 7–12.
[38] Moustaid M, Platel V, Guillet M, Reynes H, Buttay C. Modeling and test of a thermosyphon loop for the cooling of a megawatt-range power electronics converter. Int J Thermofluid 2022;13:100129.
[39] Jouhara H, Merchant H. Experimental investigation of a thermosyphon based heat exchanger used in energy efficient air handling units. Energy 2012;39:82–9.
[40] Wagner AM. Review of thermosyphon applications. 2014.
[41] Eidan AA, Najim SE, Jalil JM. An experimental and a numerical investigation of HVAC system using thermosyphon heat exchangers for sub-tropical climates. Appl Therm Eng 2017;114:693–703.
[42] Holubec I, Eng P. Flat loop thermosyphon foundations in warm permafrost. In: NT got, division AM, services PWa, and, assessment CCV, engineers CCoP; 2008. citeseerx.
[43] Mat Arifin AF. Experimental investigation of open loop thermosyphoning in evacuated tube receiver under varying heat flux. IRC; 2020.
[44] Kusuda H, Imura H. Boiling heat transfer in an open thermosyphon: report 1, an experiment with water. Bulletin of JSME 1973;16:1723–33.
[45] Fukusako S, Seki N, Yamaguchi A. Free convective heat-transfer performance of a two-dimensional open thermosyphon with heat sources of cavity dotted along vertical wall, vol. 18. Waerme-Stoffuebertrag;(Germany, Federal Republic of); 1984.
[46] Arshavski I, Nekhamkin Y, Olek S, Elias E. Conjugate heat transfer in an open loop thermosyphon. Int Commun Heat Mass Tran 1994;21:153–66.
[47] Isaac Aragones D, Chen C-H, Weibel JA, Warsinger DM, Bonner RW. Experimental and modelling analysis of a large-scale two-phase loop thermosyphon. Heat transfer summer conference. American Society of Mechanical Engineers; 2022. p. V001T13A.
[48] Lu L, Liu Z-H, Xiao H-S. Thermal performance of an open thermosyphon using nanofluids for high-temperature evacuated tubular solar collectors: Part 1: indoor experiment. Sol Energy 2011;85:379–87.

[49] Ritthong N, Thongkom S, Sawisit A, Duangsa B, Ritthong W. Optimization design of closed-loop thermosyphons: experimentation and computational fluid dynamics modeling. Energies 2024;17:527.
[50] Jafari D, Franco A, Filippeschi S, Di Marco P. Two-phase closed thermosyphons: a review of studies and solar applications. Renew Sustain Energy Rev 2016;53:575–93.
[51] Fadhl B, Wrobel LC, Jouhara H. Numerical modelling of the temperature distribution in a two-phase closed thermosyphon. Appl Therm Eng 2013;60:122–31.
[52] Alizadeh M, Ganji DD. Heat transfer characteristics and optimization of the efficiency and thermal resistance of a finned thermosyphon. Appl Therm Eng 2021:183.
[53] Noie S. Heat transfer characteristics of a two-phase closed thermosyphon. Appl Therm Eng 2005;25:495–506.
[54] Cheng G, Sun Z, Niu F. Application of the roadbed cooling approach in Qinghai–Tibet railway engineering. Cold Reg Sci Technol 2008;53:241–58.
[55] Li G, Wang F, Ma W, Fortier R, Mu Y, Zhou Z, et al. Field observations of cooling performance of thermosyphons on permafrost under the China-Russia Crude Oil Pipeline. Appl Therm Eng 2018;141:688–96.
[56] Jin M, Shang K, Yu Q, Chen K, Guo L, You Y. Study on working performance and cooling effect of a novel horizontal thermosyphon applied to expressway embankment in permafrost regions. Cold Reg Sci Technol 2024:104147.
[57] Luo X, Yu Q, Ma Q, Guo L. Study on the heat and deformation characteristics of an expressway embankment with shady and sunny slopes in warm and ice-rich permafrost regions. Transport Geotech 2020;24:100390.
[58] Lai Y, Guo H, Dong Y. Laboratory investigation on the cooling effect of the embankment with L-shaped thermosyphon and crushed-rock revetment in permafrost regions. Cold Reg Sci Technol 2009;58:143–50.
[59] Dong Y-h, Lai Y-m, Chen W. Cooling effect of combined L-shaped thermosyphon, crushed-rock revetment and insulation for high-grade highways in permafrost regions. Chin J Geotech Eng 2012;34:1043–9.
[60] Chen K, Jin M, Li G, Liu Y, Lu J, Zhao Y, Yu Q. Thermal performance and heat transfer process of an expressway embankment with horizontal-thermosyphons in permafrost regions. Cold Reg Sci Technol 2023;212:103887.
[61] Kakaç S, Avelino M, Smirnov HF. Low temperature and cryogenic refrigeration. Springer Science & Business Media; 2012.
[62] Babu NN, Kamath H. Materials used in heat pipe. Mater Today Proc 2015;2:1469–78.
[63] Ong K-S, Lim C. Performance of water filled thermosyphons between 30-150oC. Frontiers in Heat Pipes (FHP). 2015;6.
[64] Jouhara H, Robinson AJ. Experimental investigation of small diameter two-phase closed thermosyphons charged with water, FC-84, FC-77 and FC-3283. Appl Therm Eng 2010;30:201–11.
[65] Abou-Ziyan H, Helali A, Fatouh M, El-Nasr MA. Performance of stationary and vibrated thermosyphon working with water and R134a. Appl Therm Eng 2001;21:813–30.
[66] Palm Br, Khodabandeh R. Choosing working fluid for two-phase thermosyphon systems for cooling of electronics. J Electron Packag 2003;125:276–81.
[67] Ong K, Haider-E-Alahi M. Performance of a R-134a-filled thermosyphon. Appl Therm Eng 2003;23:2373–81.
[68] Handbook A. FUNDAMENTALS, MATERIALS, CHAPTER 30, thermophysical properties of refrigerants. 2009., TC 3.1.
[69] Faghri A. Heat pipe science and technology. Global Digital Press; 1995.
[70] Jouhara H, Chauhan A, Nannou T, Almahmoud S, Delpech B, Wrobel LC. Heat pipe based systems-Advances and applications. Energy 2017;128:729–54.
[71] Ong K, Hamlaoui A. Experimental observations of water-filled and R134a-filled thermosyphons operating at low temperatures. J Energy Heat Mass Tran 2002;24:235–54.
[72] Ong KS. Effects of inclination and FIll ratio on R134a and R410A. J Energy Heat Mass Tran 2011;33:145–52.
[73] Esen M, Esen H. Experimental investigation of a two-phase closed thermosyphon solar water heater. Sol Energy 2005;79:459–68.
[74] Ong K-S, Tong W, Gan J, Hisham N. Axial temperature distribution and performance of R410a and water filled thermosyphon at various fill ratios and inclinations. Frontiers in Heat Pipes (FHP). 2014;5.
[75] Yau YH, Foo Y. Comparative study on evaporator heat transfer characteristics of revolving heat pipes filled with R134a, R22 and R410A. Int Commun Heat Mass Tran 2011;38:202–11.
[76] Said Z, Rahman SM, Sohail MA, Bahman AM, Alim MA, Shaik S, et al. Nano-refrigerants and nano-lubricants in refrigeration: synthesis, mechanisms, applications, and challenges. Appl Therm Eng 2023:121211.
[77] Tian Q, Cai D, Ren L, Tang W, Xie Y, He G, Liu F. An experimental investigation of refrigerant mixture R32/R290 as drop-in replacement for HFC410A in household air conditioners. Int J Refrig 2015;57:216–28.
[78] Mota-Babiloni A, Navarro-Esbrí J, Barragán-Cervera Á, Molés F, Peris B. Analysis based on EU Regulation No 517/2014 of new HFC/HFO mixtures as alternatives of high GWP refrigerants in refrigeration and HVAC systems. Int J Refrig 2015;52:21–31.
[79] Sethi A, Becerra EV, Motta SFY, Spatz MW. Low GWP R22 replacement for air conditioning in high ambient conditions. Int J Refrig 2015;57:26–34.
[80] Mota-Babiloni A, Navarro-Esbrí J, Makhnatch P, Molés F. Refrigerant R32 as lower GWP working fluid in residential air conditioning systems in Europe and the USA. Renew Sustain Energy Rev 2017;80:1031–42.
[81] Ma L, Shang L, Zhong D, Ji Z. Experimental investigation of a two-phase closed thermosyphon charged with hydrocarbon and Freon refrigerants. Appl Energy 2017;207:665–73.
[82] Qiu J, Zhang H. Experimental investigation on two-phase frictional pressure drop of R600a and R600a/3GS oil mixture in a smooth horizontal tube. Int J Refrig 2020;117:307–15.
[83] Sengers J, Kamgar-Parsi B. Representative equations for the viscosity of water substance: American chemical society and the American institute of physics for the. 1984.
[84] Micallef D. Fundamentals of refrigeration thermodynamics. línea]. 2014. arma.org. au/wpcontent/uploads/2017/03.
[85] Zhang H, Shao S, Tian C, Zhang K. A review on thermosyphon and its integrated system with vapor compression for free cooling of data centers. Renew Sustain Energy Rev 2018;81:789–98.
[86] Samba A, Louahlia-Gualous H, Le Masson S, Nörterhäuser D. Two-phase thermosyphon loop for cooling outdoor telecommunication equipments. Appl Therm Eng 2013;50:1351–60.
[87] Ding T, Cao Hw, He Zg, Li Z. Visualization experiment on boiling heat transfer and flow characteristics in separated heat pipe system. Exp Therm Fluid Sci 2018;91:423–31.
[88] Ding T, Cao Hw, He Zg, Li Z. Experiment research on influence factors of the separated heat pipe system, especially the filling ratio and Freon types. Appl Therm Eng 2017;118:357–64.
[89] Zhang P, Shi W, Li X, Wang B, Zhang G. A performance evaluation index for two-phase thermosyphon loop used in HVAC systems. Appl Therm Eng 2018;131:825–36.
[90] Nadjahi C, Louahlia-Gualous H, Le Masson S. Experimental study and analytical modeling of thermosyphon loop for cooling data center racks. Heat Mass Tran 2019;56:121–42.
[91] Ding T, Wen Cao H, Guang He Z, Li Z. Boiling heat transfer characteristics of the R744 coolant in the evaporator of the separated heat pipe system. Int J Heat Mass Tran 2017;113:1254–64.
[92] Payakaruk T, Terdtoon P, Ritthidech S. Correlations to predict heat transfer characteristics of an inclined closed two-phase thermosyphon at normal operating conditions. Appl Therm Eng 2000;20:781–90.
[93] Wang JCY, Ma Y. Condensation heat transfer inside vertical and inclined thermosyphons. J Heat Tran 1991;113:777–80.
[94] Emami MS, Noie S, Khoshnoodi M. Effect of aspect ratio and filling ratio on thermal performance of an inclined two-phase closed thermosyphon. Iran J Sci Technol 2008;32:39.
[95] Elmosbahi MS, Dahmouni AW, Kerkeni C, Guizani AA, Ben Nasrallah S. An experimental investigation on the gravity assisted solar heat pipe under the climatic conditions of Tunisia. Energy Convers Manag 2012;64:594–605.
[96] Wu H, Liu J, Zhang X. Feasibility study on use of cellular concrete for air convection embankment on permafrost foundations in Fairbanks, Alaska. Transport Geotech 2020;22.
[97] Zhang M, Lai Y, Dong Y, Jin L, Pei W, Harbor J. Laboratory investigation of the heat transfer characteristics of a two-phase closed thermosyphon. Cold Reg Sci Technol 2013;95:67–73.
[98] Gorecki G. Investigation of two-phase thermosyphon performance filled with modern HFC refrigerants. Heat Mass Tran 2018;54:2131–43.
[99] Lataoui Z, Jemni A. Experimental investigation of a stainless steel two-phase closed thermosyphon. Appl Therm Eng 2017;121:721–7.
[100] Ong K, Goh G, Tshai K, Chin W. Thermal resistance of a thermosyphon filled with R410A operating at low evaporator temperature. Appl Therm Eng 2016;106:1345–51.
[101] Jeong S. An experimental study on heat transfer coefficients of a CO2-filled thermosyphon. Exp Heat Transf 2011;24:257–65.
[102] Terdtoon P, Chailungkar M, Shiraishi M. Effects of aspect ratios on internal flow patterns of an inclined closed two-phase thermosyphon at normal operating condition. Heat Transf Eng 1998;19:75–85.
[103] Terdtoon P, Waowaew N, Tantakom P. Internal flow patterns of an inclined closed two-phase thermosyphon at critical state: case study II, effect of Bond number. Exp Heat Transf 1999;12:359–73.
[104] Nakano A, Shiraishi M, Nishio M, Murakami M. An experimental study of heat transfer characteristics of a two-phase nitrogen thermosyphon over a large dynamic range operation. Cryogenics 1998;38:1259–66.
[105] Solomon AB, Roshan R, Vincent W, Karthikeyan V, Asirvatham LG. Heat transfer performance of an anodized two-phase closed thermosyphon with refrigerant as working fluid. Int J Heat Mass Tran 2015;82:521–9.
[106] Anand RS, Jawahar CP, Solomon AB, Bellos E. A review of experimental studies on cylindrical two-phase closed thermosyphon using refrigerant for low-temperature applications. Int J Refrig 2020;120:296–313.
[107] Sun B, Yang D. Experimental study on the heat transfer characteristics of nanorefrigerants in an internal thread copper tube. Int J Heat Mass Tran 2013;64:559–66.
[108] Mahbubul I, Fadhilah S, Saidur R, Leong K, Amalina M. Thermophysical properties and heat transfer performance of Al2O3/R-134a nanorefrigerants. Int J Heat Mass Tran 2013;57:100–8.
[109] Mahbubul I, Saidur R, Amalina M. Heat transfer and pressure drop characteristics of Al2O3-R141b nanorefrigerant in horizontal smooth circular tube. Procedia Eng 2013;56:323–9.
[110] Mahbubul I, Saidur R, Amalina M. Influence of particle concentration and temperature on thermal conductivity and viscosity of Al2O3/R141b nanorefrigerant. Int Commun Heat Mass Tran 2013;43:100–4.
[111] Mahbubul I, Saidur R, Amalina M. Thermal conductivity, viscosity and density of R141b refrigerant based nanofluid. Procedia Eng 2013;56:310–5.
[112] Kedzierski MA, Gong M. Effect of CuO nanolubricant on R134a pool boiling heat transfer. Int J Refrig 2009;32:791–9.

[113] Henderson K, Park Y-G, Liu L, Jacobi AM. Flow-boiling heat transfer of R-134a-based nanofluids in a horizontal tube. Int J Heat Mass Tran 2010;53:944–51.
[114] Jiang W, Ding G, Peng H. Measurement and model on thermal conductivities of carbon nanotube nanorefrigerants. Int J Therm Sci 2009;48:1108–15.
[115] Sabareesh RK, Gobinath N, Sajith V, Das S, Sobhan C. Application of TiO2 nanoparticles as a lubricant-additive for vapor compression refrigeration systems–An experimental investigation. Int J Refrig 2012;35:1989–96.
[116] Diao Y, Li C, Zhao Y, Liu Y, Wang S. Experimental investigation on the pool boiling characteristics and critical heat flux of Cu-R141b nanorefrigerant under atmospheric pressure. Int J Heat Mass Tran 2015;89:110–5.
[117] Akhavan-Behabadi M, Sadoughi M, Darzi M, Fakoor-Pakdaman M. Experimental study on heat transfer characteristics of R600a/POE/CuO nano-refrigerant flow condensation. Exp Therm Fluid Sci 2015;66:46–52.
[118] Zohuri B. Functionality, advancements and industrial applications of heat pipes. Academic Press; 2020.
[119] Yarmak E, Long E. Some considerations regarding the design of two-phase liquid/vapor convection type passive refrigeration systems. Proc 4th Int Conf on Permafrost, National Academy Press1984. p. 325-326.
[120] Heuer CE. The application of heat pipes on the Trans-Alaska pipeline. 1979.
[121] Wu J, Ma W, Sun Z, Wen Z. In-situ study on cooling effect of the two-phase closed thermosyphon and insulation combinational embankment of the Qinghai–Tibet Railway. Cold Reg Sci Technol 2010;60:234–44.
[122] Popov A, Vaaz S, Usachev A. Review of the current conditions for the application of heat pipes (thermosyphons) to stabilize the temperature of soil bases under facilities in the far North. Heat Pipe Science and Technology. Int J 2010;1.
[123] Varlamov SP, Skachkov YB, Skryabin PN. Evolution of the thermal state of permafrost under climate warming in Central Yakutia. Holocene 2019;29:1401–10.
[124] Zueter AF, Newman G, Sasmito AP. Numerical study on the cooling characteristics of hybrid thermosyphons: case study of the Giant Mine, Canada. Cold Reg Sci Technol 2021;189.
[125] Hayley D. Application of heat pipes to design of shallow foundations on permafrost. Proceedings of the 4th Canadian permafrost conference: Ottowa. National Research Council of Canada; 1982.
[126] Edlund J, Gordon G, Robinson P. A model mine shows its cracks. Unpublished report by Pacific Environment. 1998. [Accessed 21 May 2013].
[127] Hayley D, Seto J, Grapel C, Cathro D, Valeriote M. Performance of two rockfill dams with thermosyphons on permafrost foundations, Ekati Diamond Mine, NT. 57th Canadian geotechnical conference, Quebec City2004.
[128] Pozin V, Korolev A, Naumov M. The “ice complex” in Central Yakutia as a testing area for railway construction under extreme engineering-geocryological conditions. Inzhenernaya Geol 2009;1:15–8.
[129] Varlamov S. Temperature study of railway embankments on ice-rich permafrost in Yakutia. Journal of Engineering of Heilongjiang University Special Edition of the 10th International Symposium on Permafrost Engineering2014. p. 90-99.
[130] Permyakov PP, Zhirkov AF, Varlamov SP, Skryabin PN, Popov GG. Numerical modeling of railway embankment deformations in permafrost regions, central Yakutia. Transportation soil engineering in cold regions. Proceedings of TRANSOILCOLD 2019. vol. 2. Springer; 2020. p. 93–103.
[131] Varlamov SP. Thermal monitoring of railway subgrade in a region of ice-rich permafrost, Yakutia, Russia. Cold Reg Sci Technol 2018;155:184–92.
[132] Cao Y, Li G, Ma W, Chen D, Shang Y, Wu G, et al. Permafrost degradation induced by warm-oil pipelines and analytical results of thermosyphon-based thawing mitigation. Energy 2023;269:126836.
[133] Wang F, Li G, Alexander F, Ma W, Chen D, Wu G, et al. Applicability analysis of thermosyphon for thermally stabilizing pipeline foundation permafrost and its layout optimization. Cold Reg Sci Technol 2023;208:103769.
[134] Zhi W, Yu S, Wei M, Jilin Q, Wu J. Analysis on effect of permafrost protection by two-phase closed thermosyphon and insulation jointly in permafrost regions. Cold Reg Sci Technol 2005;43:150–63.
[135] Zhi W, Yu S, Wei M, Jilin Q. Evaluation of EPS application to embankment of Qinghai–Tibetan railway. Cold Reg Sci Technol 2005;41:235–47.
[136] Ran L, Xue X, Bao L. Applications and technical characteristics of thermal pipe subgrade in Qinghai-Tibet Railway Design. J Glaciol Geocryol 2004;26:151–4.
[137] Qingbai W, Shiyun Z, Wei M, Yongzhi L, Luxin Z. Monitoring and analysis of cooling effect of block-stone embankment for Qinghai-Tibet Railway. Chin J Geotech Eng 2005;27:1386–90.
[138] Pan W, Zhao S, Xu W, Yu S, Ma W. Application of thermal probe to enhance thermal stability of roadbed in plateau permafrost areas. J Glaciol Geocryol 2003;25:433–8.
[139] Yongping Y, Qingchao W, Shunhua Z, Luxin Z. Thermosyphon technology and its application in permafrost. Chin J Geotech Eng 2005;27:698–706.
[140] Wang G-f, Lin C, Zhu L, Feng D-c, Xin Y-y, Zhang F. Performance analyses of two-phase closed thermosyphons for road embankments in the high-latitude permafrost regions. J Mt Sci 2023;20:3138–53.
[141] Song Y, Jin L, Zhang J. In-situ study on cooling characteristics of two-phase closed thermosyphon embankment of Qinghai–Tibet Highway in permafrost regions. Cold Reg Sci Technol 2013;93:12–9.
[142] Zhang B, Sheng Y, Chen J, Li J. In-situ test study on the cooling effect of two-phase closed thermosyphon in marshy permafrost regions along the Chaidaer–Muli Railway, Qinghai Province, China. Cold Reg Sci Technol 2011;65:456–64.
[143] Wu D, Jin L, Peng J, Dong Y, Liu Z. The thermal budget evaluation of the two-phase closed thermosyphon embankment of the Qinghai–Tibet Highway in permafrost regions. Cold Reg Sci Technol 2014;103:115–22.
[144] Guo L, Yu Q, Yin N, You Y, Wang J, Sun Y, Chen K. Two-phase closed thermosyphon-induced frost jacking of piles and foundation instability in a thawed permafrost area. Nat Hazards 2024;120:619–37.
[145] Hu T, Liu J, Chang J, Hao Z. Development of a novel vapor compression refrigeration system (VCRS) for permafrost cooling. Cold Reg Sci Technol 2021;181:103173.
[146] Liu Y, Chen J, Wang C, Liu Y, Zhang S, Dong T, et al. Experimental research on the cooling effect of a novel two-phase closed thermosyphon with semiconductor refrigeration in permafrost regions. Case Stud Therm Eng 2024;54:103935.
[147] Pei W, Zhang M, Lai Y, Zhang X, Luo T. A self-adaption horizontal thermosyphon technology in uneven thermal control of roadway embankments in sub-arctic permafrost regions. Transport Geotech 2022;33:100714.
[148] Yan Z, Zhang M, Lai Y, Pei W, Luo T, Yu F, Yang S. Countermeasures combined with thermosyphons against the thermal instability of high-grade highways in permafrost regions. Int J Heat Mass Tran 2020;153:119047.
[149] Qi S, Li G, Chen D, Niu F, Sun Z, Wu G, et al. Research on the characteristics of thermosyphon embankment damage and permafrost distribution based on ground-penetrating radar: a case study of the Qinghai–Tibet Highway. Remote Sens 2023;15:2651.
[150] Qin Y, Wang T, Yuan W. Wind-driven device for cooling permafrost. Nat Commun 2023;14:7558.
[151] Cao Y, Ma W, Li G, Gao K, Li C, Chen D, et al. Rapid permafrost thaw under buried oil pipeline and effective solution using a novel mitigative technique based on field and laboratory results. Cold Reg Sci Technol 2024:104119.
[152] Guo L, Zhang Z, Wang X, Yu Q, You Y, Yuan C, et al. Stability analysis of transmission tower foundations in permafrost equipped with thermosiphons and vegetation cover on the Qinghai-Tibet Plateau. Int J Heat Mass Tran 2018;121:367–76.
[153] Pei W, Zhang M, Yan Z, Li S, Lai Y. Numerical evaluation of the cooling performance of a composite L-shaped two-phase closed thermosyphon (LTPCT) technique in permafrost regions. Sol Energy 2019;177:22–31.
[154] Chen L, Yu W, Lu Y, Liu W. Numerical simulation on the performance of thermosyphon adopted to mitigate thaw settlement of embankment in sandy permafrost zone. Appl Therm Eng 2018;128:1624–33.
[155] Pan Y, Wu C. Numerical investigations and engineering applications on freezing expansion of soil restrained two-phase closed thermosyphons. Int J Therm Sci 2002;41:341–7.
[156] Luo X, Yu Q, Ma Q, You Y, Wang J, Wang S. Evaluation on the stability of expressway embankment combined with L-shaped thermosyphons and insulation boards in warm and ice-rich permafrost regions. Transport Geotech 2021;30:100633.
[157] Pei W, Zhang M, Yan Z, Lai Y, Lu J, Dai Y. Thermal control performance of the embankment with L-shaped thermosyphons and insulations along the Gonghe-Yushu Highway. Cold Reg Sci Technol 2022:194.
[158] Yu F, Zhang M, Lai Y, Liu Y, Qi J, Yao X. Crack formation of a highway embankment installed with two-phase closed thermosyphons in permafrost regions: field experiment and geothermal modelling. Appl Therm Eng 2017;115:670–81.
[159] Lai Y, Zhang S, Zhang L, Xiao J. Adjusting temperature distribution under the south and north slopes of embankment in permafrost regions by the ripped-rock revetment. Cold Reg Sci Technol 2004;39:67–79.
[160] Feng W-j, Sun Z-z, Li G-y, Wu J. Radiation effect of shading board on embankment side slope on Tibetan Plateau. J Glaciol Geocryol 2011;28:797–808.
[161] Zhang Z, Yu Q, You Y, Guo L, Wang X, Liu G, Wu G. Cooling effect analysis of temperature-controlled ventilated embankment in Qinghai-Tibet testing expressway. Cold Reg Sci Technol 2020;173.
[162] Chen L, Voss CI, Fortier D, McKenzie JM. Surface energy balance of sub-Arctic roads with varying snow regimes and properties in permafrost regions. Permafr Periglac Process 2021;32:681–701.
[163] Shi L, Li N, Li G-y, Bi G. Stability analysis of the awning in road engineering in permafrost regions. J Glaciol Geocryol 2007;29:986–91.
[164] Yu Q, Pan X, Cheng G, He N-w. Study on main influential factors on ventilated embankment and corresponding measures. Chin J Rock Mech Eng 2007;26:3045–51.
[165] Qihao Y, Xicai P, Guodong C, Yang B. Heat transfer process of roadway embankments with different type and width of road surface in permafrost regions. Prog Nat Sci 2007;17:314–9.
[166] McFadden T. Using soil temperatures to monitor thermosyphon performance. J Cold Reg Eng 1987;1:145–57.
[167] Bayasan RM, Korotchenko AG, Volkov NG, Pustovoit GP, Lobanov AD. Use of two-phase heat pipes with the enlarged heat-exchange surface for thermal stabilization of permafrost soils at the bases of structures. Appl Therm Eng 2008;28:274–7.
[168] Chen J, Xu S, Dou S, Zhang L. Observation and study of cooling radius of heat pipes in swampy permafrost regions along Qaidar–Muli Railway. J Glaciol Geocryol 2011;33:897–901.
[169] McFadden TT. Performance of the thermotube permafrost stabilization system in the Airport runway at Bethel. Alaska: Alaska department of transportation and public facilities. Division of Planning; 1985.
[170] McFadden T. Stabilization of a permafrost subsidence in the airport runway at Bethel Alaska. Cold regions engineering. 1986. p. 118–33.
[171] An W, Wu Z, Ma W. Interaction among temperature, moisture and stress fields in frozen soil. Lanzhou, China: Lanzhou University Press; 1990.
[172] Zhang M, Pei W, Lai Y, Niu F, Li S. Numerical study of the thermal characteristics of a shallow tunnel section with a two-phase closed thermosyphon group in a

permafrost region under climate warming. Int J Heat Mass Tran 2017;104:952–63.
[173] Zhang M, Lai Y, Zhang J, Sun Z. Numerical study on cooling characteristics of two-phase closed thermosyphon embankment in permafrost regions. Cold Reg Sci Technol 2011;65:203–10.
[174] Alizadehdakhel A, Rahimi M, Alsairafi AA. CFD modeling of flow and heat transfer in a thermosyphon. Int Commun Heat Mass Tran 2010;37:312–8.
[175] Pei W, Zhang M, Li S, Lai Y, Dong Y, Jin L. Laboratory investigation of the efficiency optimization of an inclined two-phase closed thermosyphon in ambient cool energy utilization. Renew Energy 2019;133:1178–87.
[176] Chen L, Yu W, Lu Y, Wu P, Han F. Characteristics of heat fluxes of an oil pipeline armed with thermosyphons in permafrost regions. Appl Therm Eng 2021;190:116694.
[177] Liu J, Yu H. A simplified calculation method for efficiencies of circumferential fins. Energy Conserv Technol 2011;29:245–7.
[178] Lu Y, Yi X, Yu W, Liu W. Numerical analysis on the thermal regimes of thermosyphon embankment in snowy permafrost area. Sciences in Cold and Arid Regions 2018;9:580–6.
[179] Bonacina C, Comini G, Fasano A, Primicerio M. Numerical solution of phase-change problems. Int J Heat Mass Tran 1973;16:1825–32.
[180] Li S, Pei W, Wang C, Lai Y, Shi L. Thermo-seismic performances of a unilateral two-phase closed thermosyphon (TPCT) embankment in earthquake-prone permafrost regions. Transport Geotech 2021;27:100456.
[181] Lai Y, Wang Q, Niu F, Zhang K. Three-dimensional nonlinear analysis for temperature characteristic of ventilated embankment in permafrost regions. Cold Reg Sci Technol 2004;38:165–84.
[182] Lai Y, Zhang L, Zhang S, Mi L. Cooling effect of ripped-stone embankments on Qing-Tibet railway under climatic warming. Chin Sci Bull 2003;48:598–604.
[183] Tian Y, Yang Z, Liu Y, Cai X, Shen Y. Long-term thermal stability and settlement of heat pipe-protected highway embankment in warm permafrost regions. Eng Geol 2021;292:106269.
[184] Tai B, Liu J, Wang T, Shen Y, Li X. Numerical modelling of anti-frost heave measures of high-speed railway subgrade in cold regions. Cold Reg Sci Technol 2017;141:28–35.
[185] Mu Y, Wang G, Yu Q, Li G, Ma W, Zhao S. Thermal performance of a combined cooling method of thermosyphons and insulation boards for tower foundation soils along the Qinghai–Tibet Power Transmission Line. Cold Reg Sci Technol 2016;121:226–36.
[186] Li S, Lai Y, Zhang M, Yu W. Seasonal differences in seismic responses of embankment on a sloping ground in permafrost regions. Soil Dynam Earthq Eng 2015;76:122–35.
[187] Wang T, Yan L-E. A heat-flux upper boundary for modeling temperature of soils under an embankment in permafrost region. Sci Rep 2022;12:13295.
[188] Zhu L. Study of the adherent layer on different types of ground in permafrost regions on the Qinghai-Xizang Plateau. J Glaciol Geocryol 1988;10:8–14.
[189] Liu H, Niu F, Niu Y, Lin Z, Lu J, Luo J. Experimental and numerical investigation on temperature characteristics of high-speed railway's embankment in seasonal frozen regions. Cold Reg Sci Technol 2012;81:55–64.
[190] Pei W, Zhang M, Li S, Lai Y, Jin L, Zhai W, et al. Geotemperature control performance of two-phase closed thermosyphons in the shady and sunny slopes of an embankment in a permafrost region. Appl Therm Eng 2017;112:986–98.
[191] Bai R, Lai Y, Zhang M, Jiang H. Investigating the thermo-hydro-mechanical behavior of loess subjected to freeze–thaw cycles. Acta Geotechnica 2024:1–14.
[192] Song C, Dai C, Gao Y, Wang C, Yu M, Tu W, et al. Spatial–temporal characteristics of freezing/thawing index and permafrost distribution in Heilongjiang Province, China. Sustainability 2022;14:16899.
[193] Frauenfeld OW, Zhang T, Mccreight JL. Northern hemisphere freezing/thawing index variations over the twentieth century. Int J Climatol: J Roy Meteorol Soc 2007;27:47–63.
[194] Wu T, Wang Q, Zhao L, Batkhishig O, Watanabe M. Observed trends in surface freezing/thawing index over the period 1987–2005 in Mongolia. Cold Reg Sci Technol 2011;69:105–11.
[195] Lai Y, Zhang M, Li S. Theory and application of cold regions engineering. Beijing, China: Beijing Science and Technology Press; 2009.
[196] Pei W, Zhang M, Wan X, Lai Y, Wang C. Numerical optimization of the installing position for the L-shaped TPCT in a permafrost embankment based on the spatial heat control. Sol Energy 2021;224:1406–25.
[197] Yu W, Zhang T, Lu Y, Han F, Zhou Y, Hu D. Engineering risk analysis in cold regions: state of the art and perspectives. Cold Reg Sci Technol 2020;171:102963.
[198] Singh G, Bajargan G, Datta R, Ramamurty U. Deformation and strength of Ti–6Al–4V alloyed with B at cryogenic temperatures. Mater Sci Eng 2014;611:45–57.
[199] Zang MC, Niu HZ, Zhang HR, Tan H, Zhang DL. Cryogenic tensile properties and deformation behavior of a superhigh strength metastable beta titanium alloy Ti–15Mo–2Al. Mater Sci Eng 2021;817.
[200] Aftret HM, Daleng VM. Suitability of thermosyphon as a ground freezing technology in Longyearbyen. NTNU; 2022.
[201] Kane RD. Corrosion in petroleum refining and petrochemical operations. Corrosion: environments and industries. ASM International; 2006. p. 967–1014.
[202] Wang Y, Niu F, Ding Z, Wang Z. Experimental study of polyurethane cement composite–reinforced soft soil in the thawed layer in permafrost regions. Constr Build Mater 2024;420:135622.
[203] Pandis PK, Papaioannou S, Siaperas V, Terzopoulos A, Stathopoulos VN. Evaluation of Zn-and Fe-rich organic coatings for corrosion protection and condensation performance on waste heat recovery surfaces. Int J Thermofluid 2020;3:100025.
[204] Zhang J, Lin G, Vaidya U, Wang H. Past, present and future prospective of global carbon fibre composite developments and applications. Compos B Eng 2023:250.
[205] Sun Z, Luo Y, Chen C, Dong Z, Jiang G, Chen F, Ma P. Mechanical enhancement of carbon fiber-reinforced polymers: from interfacial regulating strategies to advanced processing technologies. Prog Mater Sci 2024;142.
[206] Vijayan DS, Sivasuriyan A, Devarajan P, Stefańska A, Wodzyński Ł, Koda E. Carbon fibre-reinforced polymer (CFRP) composites in civil engineering application—a comprehensive review. Buildings 2023;13.
[207] Li Y, Jin H, Wen Z, Li X, Zhang Q. Stability of the foundation of buried energy pipeline in permafrost region. Geofluids 2021;2021:3066553.
[208] Streletskiy D, Anisimov O, Vasiliev A, Permafrost degradation. Snow and ice-related hazards, risks, and disasters. Elsevier; 2015. p. 303–44.
[209] Cao J, Zheng Z, Asim M, Hu M, Wang Q, Su Y, et al. A review on independent and integrated/coupled two-phase loop thermosyphons. Appl Energy 2020;280:115885.
[210] Streletskiy DA, Shiklomanov NI, Nelson FE. Permafrost, infrastructure, and climate change: a GIS-based landscape approach to geotechnical modeling. Arctic Antarct Alpine Res 2012;44:368–80.
[211] Anisimov O, Belolutskaya M, Grigor'ev M, Instanes A, Kokorev V, Oberman N, et al. The major natural and social-economic consequences of climate change in permafrost region: a forecast based upon a synthesis of observations and modeling. Assessment report. Moscow: Greenpeace; 2010.
[212] Kondratiev VG. Geocryological problems of railroads on permafrost. Iscord 2013: planning for sustainable cold Regions2013. p. 191-203.
[213] Cluever J, Esselman T, Bruck P. Maintenance optimization: finding the best frequencies of maintenance activities. Pressure vessels and piping Conference. American Society of Mechanical Engineers; 2020. p. V008T08A29.
[214] Ran Y, Cheng G, Dong Y, Hjort J, Lovecraft AL, Kang S, et al. Permafrost degradation increases risk and large future costs of infrastructure on the Third Pole. Commun Earth Environ 2022;3:238.
[215] Sizirici B, Rachid E, Eniola JO. Assessing passive thermosyphon solar water heater as low-cost, sustainable water disinfection technology: leveraging the Germicidal effect of copper and thermal convection loops. J Environ Chem Eng 2024;12:112475.
[216] Hsu C-C, Yang D-C, Su T-W, Kuo L-S, Chen P-H. Thermal performance improvement of a cylindrical thermosyphon with modified wettability on both evaporator and condenser sections. Am J Heat Mass Tran 2014;3:104–12.
[217] Weng HC, Yang M-H. Heat transfer performance enhancement of gravity heat pipes by growing AAO nanotubes on inner wall surface. Inventions 2018;3:42.
[218] Rahimi M, Asgary K, Jesri S. Thermal characteristics of a resurfaced condenser and evaporator closed two-phase thermosyphon. Int Commun Heat Mass Tran 2010;37:703–10.
[219] Xue M, Kojima N, Machimura T, Tokai A. Flow, stock, and impact assessment of refrigerants in the Japanese household air conditioner sector. Sci Total Environ 2017;586:1308–15.
[220] Tong Z, Han Z, Fang C, Wen X. Two-phase thermosyphon loop with different working fluids used in data centers. Int J Heat Mass Tran 2023;214:124393.
[221] Longo GA, Mancin S, Righetti G, Zilio C. R1234yf and R1234ze (E) as environmentally friendly replacements of R134a: assessing flow boiling on an experimental basis. Int J Refrig 2019;108:336–46.
[222] Minor B, Spatz M. HFO-1234yf low GWP refrigerant update. 2008.
[223] J Steven Brown PhD P. HFOs: new, low global warming potential refrigerants. ASHRAE J 2009;51:22.
[224] Mota-Babiloni A, Navarro-Esbrí J, Barragán Á, Molés F, Peris B. Drop-in energy performance evaluation of R1234yf and R1234ze (E) in a vapor compression system as R134a replacements. Appl Therm Eng 2014;71:259–65.
[225] Yıldırım R. Investigation of the two-phase closed thermosyphon filled with R1234yf alternative to R134a: energy and environmental analysis. J Therm Anal Calorim 2023;148:1061–72.
[226] Kondou C, Umemoto S, Koyama S, Mitooka Y. Improving the heat dissipation performance of a looped thermosyphon using low-GWP volatile fluids R1234ze (Z) and R1234ze (E) with a super-hydrophilic boiling surface. Appl Therm Eng 2017;118:147–58.
[227] Basaran A, Ozgener L. Investigation of the effect of different refrigerants on performances of binary geothermal power plants. Energy Convers Manag 2013;76:483–98.
[228] Basaran A, Benim AC, Yurddas A. Numerical simulation of the condensation flow of the isobutane (R600a) inside microchannel. Heat Transf Eng 2021;43:337–61.
[229] Basaran A, Benim AC, Yurddas A. Prediction of heat and fluid flow in microchannel condensation. E3S web of conferences. edp sciences; 2019, 01015.
[230] Başaran A. Experimental investigation of R600a as a low GWP substitute to R134a in the closed-loop two-phase thermosyphon of the mini thermoelectric refrigerator. Appl Therm Eng 2022;211:118501.
[231] Li A, Yu B, Zhang Y, Ouyang H, Guo Z, Shi J, Chen J. The emission reduction potential and cost-effectiveness of low-GWP refrigerants in electric vehicle air conditionings. 2024.
[232] Fajar TB, Bagas PR, Ukhi S, Alhamid M, Lubis A. Energy and exergy analysis of an R410A small vapor compression system retrofitted with R290. Case Stud Therm Eng 2020;21:100671.
[233] Kumar V. Enhancing heat pipe efficacy: thermosyphon analysis. New Generation Refrigerant Transition, and Design Optimization. Department of Mechanical Engineering University of Alberta Master of Science. 2023. https://doi.org/10.7939/r3-zntw-mn29.

[234] S X, Z G. Analysis of problem based on working state testing on thermal probe. Comput Meas Control 2008:943–5.
[235] Jb C, Sj W, Jz Z, Fq X, Qin S. Research on detection technique for working state of thermal pipe along Qinghai-Tibet highway. Proceedings of the Eighth international Symposium on permafrost engineering. ShaanXi, China2009. p. 10-15.
[236] Niu F-j, Li G-y, Zhao S-p, Zhang S, Zhao Y, Jin H. Current developments of research on permafrost engineering and cold region environment: a report of the 8th International Symposium on Permafrost Engineering. Sciences in Cold and Arid Regions 2010;2:93–103.